

UNCLASSIFIED

AD NUMBER
AD876702
NEW LIMITATION CHANGE
TO Approved for public release, distribution unlimited
FROM Distribution authorized to U.S. Gov't. agencies and their contractors; Administrative/Operational Use; Sep 1970. Other requests shall be referred to Air Force Materials Lab., Wright-Patterson AFB, OH 45433.
AUTHORITY
USAFML ltr, 29 Mar 1972

THIS PAGE IS UNCLASSIFIED

20
on

AD876702

AD No. —

DDC FILE COPY

A FEASIBILITY STUDY FOR VERIFICATION OF FATIGUE RELIABILITY ANALYSIS

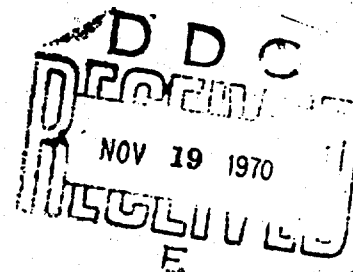
L. C. WHITTAKER

J. J. GERHARZ

THE BOEING COMPANY

TECHNICAL REPORT AFML-TR-70-157

SEPTEMBER 1970



This document is subject to special export controls and each transmittal to foreign governments or foreign nationals may be made only with prior approval of the Air Force Materials Laboratory, Wright-Patterson AFB, Ohio 45433.

W. T. G. and C. M. G. Dir.

AIR FORCE MATERIALS LABORATORY
AIR FORCE SYSTEMS COMMAND
WRIGHT-PATTERSON AIR FORCE BASE, OHIO

BEST AVAILABLE COPY

95

SPECIAL NOTICES

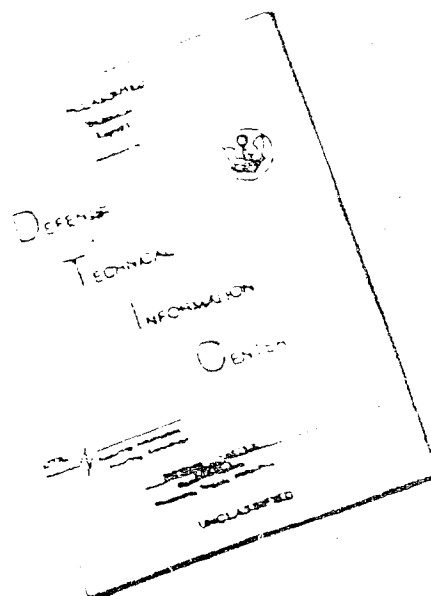
When Government drawings, specifications, or other data are used for any purpose other than in connection with a definitely related Government procurement operation, the United States Government thereby incurs no responsibility nor any obligation whatsoever; and the fact that the Government may have formulated, furnished, or in any way supplied the said drawings, specifications, or other data, is not to be regarded by implication or otherwise as in any manner licensing the holder or any other person or corporation, or conveying any rights or permission to manufacture, use, or sell any patented invention that may in any way be related thereto.

2

Copies of this report should not be returned unless return is required by security considerations, contractual obligations, or notice on a specific document.

BEST AVAILABLE COPY

DISCLAIMER NOTICE



THIS DOCUMENT IS BEST
QUALITY AVAILABLE. THE COPY
FURNISHED TO DTIC CONTAINED
A SIGNIFICANT NUMBER OF
PAGES WHICH DO NOT
REPRODUCE LEGIBLY.

REPRODUCED FROM
BEST AVAILABLE COPY

A FEASIBILITY STUDY FOR VERIFICATION OF FATIGUE RELIABILITY ANALYSIS

I. C. WHITTAKER

J. J. GERHARZ

This document is subject to special export controls and each transmittal to foreign governments or foreign nationals may be made only with prior approval of the Air Force Materials Laboratory, Wright-Patterson AFB, Ohio 45433.

The distribution of this report is limited because its scope is very limited. It contains an investigation to determine feasibility of substantiating a specialized problem of little interest to organizations not on the initial distribution.

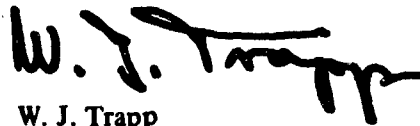
FOREWORD

The research work reported herein was conducted by The Boeing Company for the Metals and Ceramics Division, Air Force Materials Laboratory, Air Force Systems Command, Wright-Patterson Air Force Base, Ohio, under Contract No. F33615-68-C-1232. This contract was initiated under Project 7351, "Metallic Materials," Task 735106, "Behavior of Metals," with Mr. R. C. Donat acting as project engineer.

The study was conducted at The Boeing Company's Commercial Airplane Group, Structures Technology Staff, in Renton, Washington, under the supervision of Mr. J. P. Butler of the Fatigue Research Unit. The period covered by this effort is March 16, 1970 through June 15, 1970, and the report was submitted in August 1970.

The research was conducted by Mr. Ian C. Whittaker and Mr. Johann J. Gerharz of the Fatigue Research Unit of the Commercial Airplane Group. Acknowledgement is due Mr. Constantin Pavloff for his contributions to the test program, and to Dr. S. R. Varanasi for his support on the stress analysis of the panel.

This technical report has been reviewed and is approved.



W. J. Trapp
Chief, Strength and Dynamics Branch
Metals and Ceramics Division
Air Force Materials Laboratory

ABSTRACT

Experimental data have been developed and analyzed that provide some substantiation of the analytical concepts used in the fatigue reliability analysis outlined in reference 1. Extreme failure data were derived from constant-amplitude fatigue tests of large panels containing 300 identical and independent details, namely, circular holes. These tests simulate a fleet of separate details under controlled operation.

Based on finite element analyses and photoelastic experiments, an acceptable panel configuration was determined, providing a virtually identical stress field around each hole of a large number of equally stressed holes. A Boeing-developed crack monitoring system, which uses conductive paint, detected the cracks when they reached 0.02 in. in length. This permitted the cracked holes to be reworked by oversizing and cold working such that the influence on the stress fields of surrounding holes was kept at a minimum.

Estimates of the characteristic life and the log-average life were derived from constant-amplitude fatigue tests of small, single-hole specimens loaded under the same conditions as the large panels and showing a hole stress field identical to that in the large panel. These estimates were used to predict the median time to first failure in the large panel.

The constant-amplitude fatigue tests establish the feasibility of testing single specimens with a large number of identically stressed details to examine the time-to-failure distribution characteristics of the population of details.

TABLE OF CONTENTS

<u>Section</u>		<u>Page</u>
I	INTRODUCTION	1
II	TEST PROGRAM	3
III	TEST SPECIMENS	5
IV	TEST RESULTS	8
	1. Static Strain Survey	8
	2. Fatigue Test Results	8
V	DISCUSSION OF TEST RESULTS	11
	1. Static Strain Survey	11
	2. Fatigue Test Results	12
VI	CONCLUSIONS AND RECOMMENDATIONS	17
	APPENDIX—STATIC STRAIN SURVEY DATA	45
	REFERENCES	87

LIST OF ILLUSTRATIONS

<u>Figure</u>	<u>Title</u>	<u>Page</u>
1	Multihole Panel Mounted in the EMR 150,000-Lb Programmed Fatigue Testing Machine	18
2	Panel 1—Location of Strain Gages and Photoelastic Coatings	19
3	Panel 2—Location of Strain Gages	20
4	Typical Section Showing Crack-Detection Circuits	21
5	Detail of Crack-Detection Circuit Around a Single Hole	21
6	Location of Small Specimens Cut From Panel 3	22
7	Multihole Panel	23
8	Single-Hole Specimen	24
9	Computed Stress Variation for Panel With Constant Cross Section	25
10	Computed Stress Variation for Panel With Slots in the Grip Area	26
11	Computed Stress Variation for Panel With Rectangular Doublers	27
12	Computed Stress Variation for Panel With U-Shaped Doublers (Final Configuration)	28
13	Panel 2—Hole Field	29
14	Photoelastic Coating at Lower Right of Panel 1	30
15	Photoelastic Coating at Central Portion of Panel 1	30
16	Typical Strain Gage Data During Loading and Unloading	31
17	Percent Difference of Strain in Y-Direction Between Vertical Centerline and Edge of Panel	32
18	Difference in Strain Gage Readings Between Gages on the Vertical Centerline and Near the Panel Edge	33
19	Strain Gage Data of Gages Next to Cold-Worked Holes	34
20	Location of Fatigue Cracks on Panel 1	35
21	Location of Fatigue Cracks on Panel 2	36

LIST OF TABLES

<u>No.</u>	<u>Title</u>	<u>Page</u>
1	Results of a Finite Element Stress Analysis for a Strip of Aluminum Containing a Single Row of Holes Parallel to the Load Direction	37
2	Results of a Photoelastic Stress Survey With a Single- Row, Three-Hole Model Loaded Parallel to the Row of Holes	37
3	Photoelastic Stress Data at Lower Right Location—Static Load of 144,000 Lb	38
4	Single-Hole Specimen Fatigue Test Results	39
5	Panel 1—Fatigue Test Results	40
6	Panel 2—Fatigue Test Results	41
7	Statistical Parameters of Single-Hole Specimen Data	42
8	Comparison of Predicted Time to First Failure in 300 Details and the Multihole Panel Test Results	43
9	Comparison of Distribution Parameters Obtained From the Single-Hole and Multihole Test Specimens	44

SECTION I

INTRODUCTION

The variability of material or structure basic fatigue performance is one of the primary problem areas in a reliability analysis of a fatigue-critical structure. Thus, like methods for cumulative fatigue damage analysis, it is a source of continuous investigation. Recently, two well-known distribution models were used to apply reliability analyses to the fatigue analysis task. Use of the considerable available fatigue test data on aluminum alloys resulted in demonstrating the probable existence of distribution parameters that typify fatigue variability (ref. 1). Based on a knowledge of the distribution shape parameter, a fatigue reliability analysis method was developed and shown to have some potential. However, the effectiveness of the proposed method cannot be fully evaluated because of a lack of either controlled fleet fatigue performance data from service use or identical laboratory fatigue tests on very large groups of details.

Although large fleets of both military and commercial aircraft do exist, the individual aircraft are exposed to variable or different operational programs or do not have environmental load monitoring for each aircraft. Apparently neither the military nor commercial service data are sufficiently identified or cataloged so that loading conditions for each individual reported fatigue-critical detail can be precisely defined. Furthermore, laboratory test data for groups as large as a few thousand identical details are unavailable.

It therefore appears essential to develop and to analyze suitable experimental data that simulate controlled fleet operation. Toward this goal, a test of a large panel with many identical and independent details, such as circular holes, was conceived. Subjecting such a multihole panel to simple tension-tension, constant-amplitude, fatigue cycling, reflecting for example an airplane's ground-air-ground stress cycle, exposes all the holes to essentially the same environmental loading, thereby providing the control not available currently. Successive detection and removal of initiated cracks in the individual holes for the first few occurrences during the fatigue test of the panel could provide technical data suitable for evaluation by a reliability analysis.

Section II outlines the fatigue testing that was conducted to evaluate the feasibility of the program outlined in the preceding paragraph. Brief descriptions of the fatigue testing equipment and the crack detection system are also presented.

Section III describes the multihole test specimens and the results of the analytical work accomplished toward selection of the chosen configuration of the specimens.

Section IV presents the experimental results obtained from the test program and includes the results of the static strain survey and the fatigue test.

Section V discusses the experimental results and their suitability as data for verifying a reliability analysis method.

Finally, section VI lists the conclusions arrived at and presents a few recommendations.

The appendix contains tables of strain gage locations and strain results during static testing of both multihole panels.

SECTION II

TEST PROGRAM

The goal of the major experimental phase of the program was the exposure of a large number of identical and independent details to a known or controlled loading environment. Regardless of actual test-machine loading, the test of a single large panel containing many identical holes provided some consistency in load exposure for each individual hole. This phase of the experiment can be considered to be a model of a closely controlled or monitored fleet of aircraft. The mean fatigue performance was determined by subjecting small single-hole specimens to a loading history similar to that of the large panel. Consistency in manufacturing control was maintained by fabricating the small specimens from one of the large panel specimens. To maintain simplicity in the loading environment, the tests were conducted under a constant-amplitude, tension-tension fatigue load. This simulated an idealized ground-air-ground cycle stress range of an aluminum alloy wing lower surface region.

Two large, 144 by 48 by 1/8-in., 2024-T3 sheet, multihole panels were tested in an Electro Mechanical Research (EMR) programmed fatigue testing machine, figure 1. This machine has a maximum load capacity of $\pm 150,000$ lb at a frequency range of 0.5 to 20 Hz and it can accommodate specimens up to 180 in. long. The machine operates on the hydraulic servovalve closed-loop principle, and random loading is accomplished by use of a seven-track digital magnetic tape programmer. The constant-amplitude and programmed loads approximate a square wave at low frequencies and a reversed exponential wave at high frequencies. A function generator provides sinusoidal wave shape, constant-amplitude loading. Resolution of 100 lb for constant-amplitude loading and 300 lb for programmed loading is attainable. The loading range used for the test was a minimum of 6,000 lb to a maximum of 144,000 lb, corresponding to a gross stress range of 1 to 24 ksi at a cyclic frequency of 200 cpm, using a reversed exponential wave shape.

Prior to and on completion of fatigue cycling, each panel was loaded statically from zero to 24 ksi in increments of 4 ksi for both the loading and unloading portions of the load cycle. The first panel was instrumented with 19 axial strain gages, four rosette strain gages, and two photoelastic coatings, each 9 in. wide and 9 in. long. The location of these gages is shown on figure 2 and their coordinates are tabulated in the appendix, together with the static results. Three static load cycles were applied to panel 1 prior to fatigue cycling, and one single loading cycle was applied on completion of the fatigue test. Strain readings were taken and recorded on all four cycles, whereas the photoelastic coating was read only at the maximum load condition of the first cycle. The second panel was equipped with only 12 strain gages, as shown in figure 3 and tabulated in the appendix. Two loading cycles prior to, and a single load cycle on completion of, fatigue testing were applied to the panel; the strain gage readings were recorded and are presented in the appendix.

After applying the three static load cycles on panel 1, the two photoelastic coatings were removed, the panel was cleaned locally, the crack detection circuitry was completed, and fatigue cycling was begun. A Boeing-developed crack-monitoring system that uses conductive-paint crack-detection circuits was used on this test program. Twenty circuits

were used on each panel to monitor both faces of the panel; figures 4 and 5 illustrate a typical nine-hole section on the panel and the detail around a single hole, respectively. The 20 circuits were wired into a visual and audible alarm system so that initiation of a crack would break the applicable circuit and trigger the alarm. At this occurrence, the test machine was switched off, the broken circuit identified, and the location of the cracked hole determined. The existence of a crack in the hole was verified, under load, using a red dye penetrant (VP30 from the Met-L-Check Company), D-70 developer from the same company, and a 14-power hand-held magnifier. If the hole was cracked, the crack length was measured and then the hole reamed oversize to remove all traces of the crack. The oversized hole was then cold worked to prevent any further cracking at that location, and the broken detection circuit was repaired. Fatigue cycling was then restarted and continued until the next occurrence of a circuit break when the procedure just described was repeated. On a few occasions, burrs on the drill exit face of the panel initiated failures in the painted circuits without any corresponding cracks in the panel. The operational procedure at these times was simply to repair the broken circuit and then to continue cycling to the next positive indication of a crack. After obtaining the initial 22 failures on the first panel in this manner, the fatigue test was stopped and a final static loading cycle applied.

The procedure for the second panel was a repeat of that just described for panel 1, except that no photoelastic coatings had to be removed, and the initial 30 failures were obtained prior to stopping the fatigue test.

Finally, a third panel, which had been drilled on a numerically controlled machine in a manner similar to the other two panels, was cut up into 20 small single-hole specimens. The locations of these specimens with regard to the overall panel are shown in figure 6. These specimens were provided with crack-detection circuits as on the two multihole panels and were fatigue tested at a constant cyclic stress of 12.5 ± 11.5 ksi. The fatigue machine was a Sonntag Model SF-10-U, a constant-dynamic-force, inertial-compensating, mechanical-oscillator-type machine. Dynamic loading is a sinusoidal load superimposed on the static mean load by a synchronous motor rotating an adjustable eccentric mass. Flexure plates are incorporated to allow motion only in the vertical direction. The test was conducted with a 2:1 multiplier head replacing the standard head; with this head installed, machine capacity was increased to $10,000 \pm 10,000$ lb. Cyclic frequency was a constant 30 Hz. The crack-detection circuits on the specimens were wired to the test machine so that, at initiation of a crack, the machine was switched off. As before, the holes were inspected for a crack using dye penetrant, and positive indications were measured and their lengths and cyclic lives recorded. The specimens were then cycled to final failure.

SECTION III

TEST SPECIMENS

For the multihole panel, a configuration was chosen that provides a maximum number of holes surrounded with complete identical stress fields. As shown in figure 7, the 1/8-in.-thick, 48- by 144-in. panel contains 300 holes arranged in a matrix of 15 columns and 20 rows in the central portion of the plate. The 3/16-in.-diameter holes are equally spaced 3.2-in. apart (≈ 17 diameters) between the rows and columns. The edge margin of the holes in columns 1 and 15 is 8.5 diameters, and rows 1 and 20 are about 7/10 of the plate width from the grip. At the grip ends, 1/16-in.-thick doublers have been bonded to the plate on both sides. The configuration of the single-hole specimen was chosen to obtain a stress concentration factor equal to that of the identically stressed holes of the multihole panel. As shown in figure 8, these specimens are 4 in. wide and contain a 3/16-in. hole in the center.

At the present time, a closed-form solution for the stress analysis of a multihole panel is not possible, and a computational solution for the panel including the holes is impractical. The two primary parameters in the analysis are:

- Interaction of holes on each other and of holes and boundaries
- Constraint imposed by the stiff grips

These parameters were considered separately in an effort to find an optimal multihole panel configuration. Some initial exploratory work was performed on both subjects using a three-node, constant-strain, finite-element, computer program and a photoelastic model. The computer program is capable of analyzing the stress and deformation of two-dimensional structures subjected to in-plane loads and displacements and uses stress-strain response characteristics of the structural materials. Related to hole interaction effects, this study revealed the following results:

- In an infinite plate containing a matrix-like array of regularly spaced holes of the same size and subjected to a tensile load parallel to the line or column of holes, the maximum stress and stress concentration factor at the end holes may approach that of the interior holes, depending upon the spacing between holes. This difference can be reduced by either increasing the distance between the first and second holes or by enlarging the end hole. However, when applied to a finite-width strip, this latter approach becomes less valid, as the maximum stress at the end holes increases upon enlarging its size, because the net section is reduced.

To explore this interaction effect between the first and second holes along the load direction and the distance between the first hole and the grip, studies were made on the simplest specimen envisaged, namely, a strip of aluminum sheet, rigidly gripped at the ends, and containing a single line of holes parallel to the axial load.

- Some results obtained from the investigation are presented in table 1. The parameters that were varied were the grip distance to the first hole and the distance between the first and second holes. It is noted from these results that increasing the distance to the first hole from five to nine diameters lowered the ratio of the stress concentration factors K_{T1}/K_{T2} (table 1) by about 1%. However, increasing the distance between the first and second hole from four to six hole diameters lowered the ratio of the stress concentration factors by about 2%.

- An experimental check of this finite element solution was obtained from results of a photoelastic study made available from the Boeing Scientific Research Laboratories (ref. 2). A specimen 0.132 in. thick, 2.5 in. wide, and containing a single row of three holes spaced 1.5 in. apart was the model. This specimen was axially loaded in tension, and variations in peak stress differentials were obtained by varying the diameters of the central and outer holes, respectively. Table 2 summarizes the results of this experiment. Again, as noted in the preceding numerical study, it was observed that a reduction in distance between the first and second holes caused an increase in peak stress differential. It is also interesting to note, from an examination of cases 1 and 2 in tables 1 and 2, that the predicted peak stress differential is very similar to the values that were measured experimentally.
- In a semi-infinite plate containing the same array of holes, with the rows of holes parallel to the plate edge and subjected to a tensile load also parallel to the plate edge, the stress concentration factor for the edge holes may approach that of the interior holes, depending on the edge margin. This difference will approach zero with increasing spacing and edge margins. The mathematical solution of Mindlin (ref. 3) for a semi-infinite plate with a hole near the plate edge and the solution of Schoultz (ref. 3) for an infinite plate with a single row of holes perpendicular to the load direction reveal a difference in the stress concentration factors for the hole near the edge and the interior holes of approximately 1% or less for ratios of hole distance to hole diameter larger than 13 and for ratios of edge distance to hole diameter larger than 6.5.

Having demonstrated the feasibility of obtaining practically interaction-free details within a single multihole specimen—about 1% variation in peak stress for the given ratios of hole spacing to hole diameter and edge distance to hole radius of 13—it was decided to examine the effect of Poisson's ratio on the peak stress distribution. As before, a flexible sheet panel, rigidly constrained at the ends by stiff grips, was considered as the test specimen. No holes were included in this case as it was computationally impractical. Symmetry of the specimen also reduced the size of the program by modeling only a quarter plate section of the test specimen.

The chosen grid of 24 by 32, standard, three-node, constant-strain, triangular elements and results of the computer analysis are presented in figures 9 through 12 for four grip configurations. In the areas of larger stress gradients in the vicinity of the grips, a finer grid would result in a more accurate stress evaluation. The numbers written on the elements are the percentage differences in individual element equivalent stress and the average equivalent stress of the elements along the horizontal centerline (i.e., the number +2 means a stress increase between 1.5% and 2.5%; in the shaded areas, the stress change is between -0.5% and +0.5%). The coordinate stresses σ_x , σ_y , and τ_{xy} ; principal stresses σ_1 , σ_2 , and τ_{max} ; and equivalent stress based on the distortion energy (v. Mises and Hencky) have been calculated for each element and nodal point of the plate. The equivalent stress has been taken as the measure of the stress field variation over the panel, the variation is shown in figures 9 through 12.

Figure 9 shows the stress variation derived for a plate with constant cross section over the whole plate length and an initial displacement put directly on the plate in the grip area. Figure 10 shows the stress variation derived for a plate with constant width but containing

six equally spaced 16-in.-long, 3/16-in.-wide slots at the grip end parallel to the load direction and an initial displacement put directly on the plate in the slotted grip area. Figures 11 and 12 show the stress variations derived for similar plates as in figure 9 but with rectangular doublers and U-shaped doublers, respectively, bonded to the plate on both sides of the grip ends. Here the initial displacement was placed on the doublers as the calculation of the load transfer over the bond elements to the plate is incorporated in the computer program.

As a result of these computations, it was decided that a maximum of 300 holes per panel, 3/16 in. in diameter, was acceptable. By arranging these holes as shown in figure 7, a spacing of slightly more than 17 diameters is obtained. A picture of the hole field of panel 2 is shown in figure 13. This matrix of holes is located over the central area of the panel, and it is expected that only 10% of the holes will be in areas with as much total stress variation as 5%. In this context, total stress variation is the difference in equivalent stress level between the hole in the area with the lowest and the hole in the area with the highest equivalent stress. These percentages apply only to the plate with the bonded U-shaped doublers. However, for a panel with rectangular doublers, 25% of the holes would be in areas with a 6% stress variation, and if the doublers would be left off 16% of the holes would be in areas with a 4% stress variation and 17% of the holes in areas with a 5% stress variation for the panel with the slotted grips and the panel with constant cross section, respectively. The final choice, consequently, was the plate with the bonded U-shaped doublers shown in figure 12.

As a result of a comparison of the stress concentrations around the intermediate holes of the multihole panel and the hole in the single-hole specimen, the combination of a 3/16-in.-diameter hole with a 4-in. width was found acceptable for the small specimen. Based on reference 3 and the foregoing study, the stress concentration is assumed to be about $\sigma_{\max}/\sigma = 3.0$, with less than 1% difference between the intermediate and the single hole.

The material used for fabricating the specimens was 2024-T3 bare aluminum alloy, 0.125 in. thick, purchased from Reynolds heat H/T lot KH 17273-0. Two multihole panels and 20 single-hole specimens were fabricated, per figures 7 and 8, on a numerically controlled drilling machine using first a No. 15 (0.180-in. diameter) Nu Con 77 drill at 2400 rpm and finishing with a 0.187-in.-diameter reamer at 600 rpm.

Multihole panels 1 and 2 were unaltered from their original purchased size. The single-hole specimens were cut out from a third panel per figure 6 after all holes had been drilled. The 3/16-in.-diameter holes drilled in multihole panel 1 and in the single-hole specimens were left as drilled, with the burrs at the hole edges projecting from the drill exit face. Panel 2, however, was lightly sanded along each column of holes in the longitudinal direction on both sides, using 600-grit sandpaper backed by a flat steel block. Any trace of burrs projecting from the faces was removed by this operation. This was required because the primer for the liquid paint wires could not adhere to the edge of burred holes due to the slight lips at unsanded hole edges.

SECTION IV

TEST RESULTS

1. STATIC STRAIN SURVEY

a. Photoelastic Coating

Panel 1 was equipped with two 9- by 9-in. photoelastic coats at the locations shown in figure 2. Readings were taken at maximum load on the first static loading cycle. Considering first the lower right location, readings were taken at points 1 through 4. Point 1 was equidistant between the two holes on rows 18 and 19 and along column 13. Point 2 was diagonally equidistant between the four holes on rows 18 and 19 and on columns 13 and 14. Point 3 was equidistant between the two holes on row 19 and columns 13 and 14. Finally, point 4 was located equidistant between column 15 and the edge of the panel and between rows 18 and 19. This is illustrated in figure 14, and the representative stress values are given in table 3. The results of the photoelastic coating near the panel's central area are shown in figure 15. The readings showed a uniform stress distribution and consequently were not recorded.

b. Strain Gage Results

The complete set of strain gage results are tabulated in the appendix, and the information contained in this section has been limited to these data in reduced form. A typical stress-strain curve showing the strain gage data during loading and unloading is presented in figure 16. The data points correspond to average strain at the load steps of the second and third static test cycles given by strain gage 1 on panel 1 (see the appendix).

A consistent difference in strain between all gages placed along the vertical plate centerline and the gages located near the panel edge was noticed. The corresponding average percent differences at the different y-locations shown in figure 17 are based on the calculated strain and are compared to the finite element computer analysis results. Stress-strain curves that represent the average of four strain gages on the vertical centerline and the average of eight strain gages near the plate edge of panels 1 and 2, at the location $y = 109$ in., are shown in figure 18.

Strain gage data that were read before and after the fatigue test from gages 13 and 23, which were next to the cold-worked holes, are shown in figure 19. Gage 23 was located between holes 20-1 and 20-2, of which hole 20-1 had developed a fatigue crack and was reworked to 3/8-in. diameter. Gage 13 was located next to hole 1-8, which had developed a second fatigue crack after the normal repair procedure and was consequently oversized and cold worked again to a final diameter of 0.567 in.

2. FATIGUE TEST RESULTS

a. Single-Hole Specimens

Twenty single-hole specimens were fatigue tested, and their cyclic lives to the first observed crack and to final failure were both recorded. The specimens were all tested in the same test machine, and the results have been tabulated in the order of testing sequence in

table 4. The designation of left or right side of the hole applies when looking at the drill-entry face of the specimen.

b. Multihole Specimens

The results of the fatigue test on panel 1 are tabulated in table 5 and illustrated on figure 20. As before, the designation of left or right side of the hole applies when looking at the drill-entry face on the panel. The hole at row 19, column 2 and that at row 13, column 12 had cracks of 0.04 in. and 0.05 in., respectively, when first detected. The burrs at these two holes prevented locating crack detection circuits closer to the edges of the holes to allow observation of shorter cracks. During drilling of the panel, slight gouging of the panel occurred at two locations on the drill entry face as a result of incomplete raising of the drill head. A shallow horizontal gouge connected the two holes on row 3 at columns 14 and 15. Hole 3-15 also had a small vertical gouge. A fatigue crack resulted along the gouge at hole 3-14. On detection at 20,500 cycles, the crack was 0.06 in. long. The hole on row 2, column 15 was also gouged, with a shallow horizontal gouge extending from the left side of the hole approximately half way to the adjacent hole. It should be noted that this hole was the location of the first failure at 18,768 cycles; the crack initiated on the right side of the hole. At 26,901 cycles, the hole at row 1, column 8, which had been reamed out and cold worked earlier at 24,060 cycles, developed a further crack. After reworking this hole, it was decided that the final oversized hole was sufficiently large at 0.567 in. to interfere with the adjoining holes. Consequently, these adjacent holes at row 1, columns 7 and 9 and row 2, columns 7, 8, and 9 were all cold worked to circumvent any further cracking in this area. Fatigue cycling was terminated on panel 1 at 28,788 cycles after crack initiation at hole 13-9.

The fatigue test results from panel 2 are tabulated in table 6 and illustrated on figure 21. The hole at row 15, column 10 was badly deformed during drilling and subsequently was reamed oversize and cold worked prior to any fatigue cycling. On this panel, both faces were sanded smooth prior to (and to facilitate) installation of the crack-detection circuits. Fatigue cycling was terminated after 40,423 cycles had been accumulated on the panel and 30 cracks had been initiated.

SECTION V

DISCUSSION OF TEST RESULTS

1. STATIC STRAIN SURVEY

The results of the photoelastic coating on the first panel showed that, within the accuracy limitations of the technique, a uniform stress distribution existed at both areas on the panel. It should be recalled that these were 9- by 9-in. squares only, resulting in a fairly localized stress survey. However, the axial and rosette strain gages were widely distributed over the panel and did show a nonuniformity in the strain distribution across the width of the panel. Referring to the strain results given in the appendix and to the typical reduced data presented in figures 16 and 18, it can be seen that both panels exhibited the same strain behavior and were both symmetrically loaded over the panel width and thickness. Consider first the horizontal centerlines of the panels. The gages located toward the edges of the panels between the first and second and the fourteenth and fifteenth columns of holes showed an average level of strain that was 2.6% higher than the gages at the centers of the panels. This same trend was maintained throughout the area of the panels that contained the matrix of holes. For example, an average 2% variation in strain was measured at the first row of holes and an average 2.6% variation at the twentieth row. It was also confirmed that the strain variation across the panel width then increased as the bonded doublers were approached. This information has been summarized on figure 17, which also lists, for comparison, the expected stress variations predicted by the finite element analysis.

Referring to figure 17, it can be seen that an acceptable correlation between predicted and measured variation existed at the top and bottom rows of holes. However, along the horizontal centerline, the average measured variation of 2.6% was rather unexpected as the finite element solution shows a uniform stress distribution. The reason for this discrepancy is not clear at this time but may be a result of the idealization of the panel or of the accuracy in the strain gage readings, which were $\pm 2\%$. It had been assumed that the bonded doublers on the ends of the panel had a constant positive displacement across their width. The test machine, however, was equipped with friction grips, and it is conceivable that a uniform displacement was not achieved. More importantly, strain variations of this amount are within tolerable bounds and so should not unduly prejudice the ensuing fatigue results.

Finally, figure 19 compares the behavior of strain gages adjacent to holes that developed cracks during fatigue cycling. Both gages were on panel 1. Gage 23 was located at row 20 between the holes in columns 1 and 2. During cycling, a crack developed at hole 20-1 at 27,205 cycles. This hole was then typically oversized and cold worked to a final diameter of 0.38 in. Figure 19 shows gage 23 results taken before and after cyclic testing. It can be seen that the readings are virtually identical, and no apparent interference resulted from reworking an adjacent hole. Gage 13 was located at row 1 between the holes in columns 8 and 9. At 24,060 cycles, hole 1-8 developed a fatigue crack and was reworked to a diameter of 0.38 in. However, at 26,901 cycles, another fatigue crack was discovered in the repaired hole. After re-oversizing and cold working, the final hole was 0.567 in. in diameter. This was larger than the 0.38-in.-diameter limitation that had been defined for reworked holes and was believed to be of a size to cause local interference. This belief was verified at the end of the fatigue test when the gage was read. Figure 19 shows a marked difference in the gage 13 readings before and after fatigue cycling. It should be noted that this was the only occurrence on this program when a repaired hole exceeded the 0.38-in.-diameter size restriction.

2. FATIGUE TEST RESULTS

a. Single-Hole Specimen Results

The fatigue results on the small specimens were summarized in table 4. From these results it was noted that 14 of the 20 cracks initiated on the drill-exit side. As mentioned previously in section III, the small specimens were cut from a large panel that had been left as drilled, with no attempts at burr removal. Therefore, the preponderance of the failures on the exit side was not really surprising. More to the point, however, was the order in which the failures occurred. For example, there were four exit-side failures prior to the first entry-side failure; seven more exit-side failures preceded the second entry-side failure. No recognizable variation in the propagation times to failure between the drill entry and exit sides was observable. Times to a 0.02-in. crack lay in the range 65% to 85% of life to failure, with the average value falling at 73% of failure life. This value is consistent with the data published in reference 4, considering the differences in material thickness, specimen geometry, etc.

The fatigue test data were analyzed to obtain necessary statistical information. As in reference 1, the log-normal and Weibull distributions were considered, and the maximum likelihood unbiased point estimates of the shape and scale parameters were obtained. These estimates were summarized on table 7. It was obvious that the scatter in the test results was of a low order, typical of closely controlled laboratory testing where a single heat of material was used in conjunction with closely monitored testing procedures. The exit-side failures were analyzed separately from the entry-side failures because of the bias toward the exit side and for comparison with the panel results. It can be seen from the results that, depending on the statistical model used, there was a 7% to 10% difference on the average between the exit and entry sides. It was also noted during analysis that scatter of the results based on life to failure was somewhat lower than the already low scatter of the 0.02-in. crack-initiation times. This was not entirely unexpected as it seems quite likely that small variations in the 0.02-in. crack length must exist in the data and be reflected as larger scatter.

b. Multihole Panel Results

Panel 1, as in the case of the single-hole specimens, was left in the as-drilled condition with visible burrs at the hole edges on the drill-exit face. Not unexpectedly, more than two-thirds of the fatigue cracks initiated at the drill exit face. Moreover, only four cracks initiated on the inside edges of the holes, i.e., growing towards the vertical centerline of the panel. These results are tabulated on table 5, and the failure locations are shown in figure 20. Referring to this figure, note that there were seven pairs of adjacent failures. Two pairs were horizontally adjacent at row 7, columns 11 and 12 and at row 19, columns 4 and 5. A single pair at rows 13 and 14, column 1 were vertically adjacent and four pairs were diagonally adjacent. These were holes 3-1 and 4-2, 8-14 and 9-15, 19-2 and 20-1, and finally 2-15 and 3-14. Furthermore, this last pair—the first and third recorded failures—were, as mentioned in section IV, at a location that had been slightly gouged during the drilling of the holes. Other than these two holes, only one other hole (3-15) was gouged and this did not suffer a failure. Because of the uncertainties of these gouged holes, their results were discounted.

The first point about the results that was immediately obvious was that lifetimes were considerably lower than those obtained from the single-hole specimens. In fact, all 20 failures on the panel had been obtained within 80% of the lifetime of the weakest of the

single-hole specimens. Putting this another way, the average life of the panel failures was approximately half of the average life of the single-hole failures. This would seem a definite substantiation for the argument that the numerical size of the exposed sample (or fleet) be a major consideration in structural fatigue reliability analyses.

Panel 2 was, as mentioned in section III, sanded lightly on both faces to eliminate the surface burrs caused by the drilling operation. Consequently, this panel was different from either panel 1 or the single-hole specimens in that there was no observable surface variation between the drill entry and exit faces, so all failures were considered as entry-side failures. Fatigue results are listed on table 6 and the failure locations are shown in figure 21. Referring to the table and the figure, it can be seen that there were 11 pairs of adjacent failures out of the 30 recorded failures. One pair was horizontally adjacent, four pairs were adjacent in the vertical plane, and the remainder were paired diagonally. Of the 30 cracks, 21 initiated on one face of the panel and 17 were on that side of the hole nearer the edge of the panel. The apparent bias of the failures toward a single face was unexplained since both faces had been finished similarly during the sanding process. Nevertheless, it was notable that all the failures on panel 2 had occurred at a cyclic life lower than the lowest recorded entry-side failure of the single-hole specimens. This supports the trend noted in the first panel fatigue results. In summary:

- Single-hole specimens:
Lowest exit-side failure (14 data points) = 37,000 cycles
- Panel 1:
Lowest recorded exit-side failure (15 data points) = 19,504 cycles
- Panel 1:
Highest recorded exit-side failure (15 data points) = 28,788 cycles
- Single-hole specimens:
Lowest entry-side failure (6 data points) = 41,000 cycles
- Panel 1:
Lowest recorded entry-side failure (5 data points) = 24,060 cycles
- Panel 1:
Highest recorded entry-side failure (5 data points) = 27,750 cycles
- Panel 2:
Lowest recorded entry-side failure (30 data points) = 28,615 cycles
- Panel 2:
Highest recorded entry-side failure (30 data points) = 40,423 cycles

This experiment, because of its highly laborized nature, where a single heat of material was used for the fabrication of similar specimens, which were then carefully monitored while being subjected to identical loading histories, resulted in a level of scatter predictably lower than that typifying normal aluminum aircraft structure. Hence, the reliability procedure defined in reference 1 is applied to this study, but it uses the point estimates of the parameters given by experimental data obtained in this study. Therefore, based on these parameters, a reliability analysis was conducted using the single-hole specimen results to predict the median time to first failure of 300 identical and equivalent details. This prediction could then be compared to the tested performance of the multihole panels. Table 8 is a summary of the results of this computation, and it can be seen that the use of the Weibull model and a specification of median reliability of the weakest was sufficient to

predict the first failure in panel 1 and almost adequate for panel 2. Furthermore, the Weibull predictions were consistently closer than those given by the log-normal model. It should be added that the choice of the reliability level was an arbitrary selection for use in the examples just presented.

In an effort to demonstrate the type of results that would have been obtained from direct application of the values given in reference 1, it was assumed that only one single-hole specimen had been tested. This would define the scale parameter and it would be necessary to assume that scatter would be that which was typical of aluminum alloys. The average value of the 20 specimens was used as the single test result, and predictions of median time to first failure in a group of 300 details were made. The predicted lives given in table 8 show that both the Weibull and log-normal distribution models gave rather conservative answers.

Consider now the results from the first multihole panel. As shown on table 5 and figure 20, there were 15 failures on the exit face of the panel, three of which initiated at holes adjacent to previously reworked holes. These were at row 20, column 1; row 7, column 12; and row 19, column 4. Because of the possibility that the failures at these holes had been influenced by the adjacent prior failures, they were discounted from the ensuing analysis. The variation in strains across the panel noted during the static strain gage survey was assumed to have negligible effect on the fatigue performance of the individual holes. As in the case of the single-hole specimens, these 12 failure results were considered as part of a censored sample, and unbiased maximum-likelihood estimates of the shape and scale parameters were calculated and are shown on table 9.

Panel 2 had 30 recorded failures; from table 6 and figure 21 it can be seen that 10 were at adjacent holes. Following the arguments just forwarded in the previous paragraph, these 10 cracks were discounted and the remaining 20 data points were considered in the censored sample used in obtaining the unbiased shape and scale parameters.¹ These are given in table 9.

It is immediately apparent from these comparative studies that the assumption of the Weibull distribution results in an estimate of the shape parameter that was the same whether the data be of the extrema type, as obtained from the multihole panels, or of central tendency type exemplified by the single-hole specimens. Furthermore, from the published work in reference 5, it was expected that the average life of the panel holes, tested at a cycle frequency of $3\frac{1}{2}$ Hz would be lower than that of the single-hole specimens, which were cycled at 30 Hz. This expected behavior was indeed the case as predicted by the Weibull estimates of characteristic lives.

However, the assumption of log-normality for fatigue data results in quite different answers. Here it was noted that the estimate of the shape parameter was very sensitive to the type of data, the shape parameter obtained from extrema data of the panels being about twice the value given by the single-hole specimens. Furthermore, the mean lives predicted for both panels were noted to be higher than their single-hole equivalents instead of the opposite trend, which was expected.

¹ However, omission of these adjacent crack locations on both panels does increase the mean or characteristic life and the bounded values to some degree.

Based on the results of this specific investigation, it would appear that the Weibull model is better suited to handling extrema data, because consistent estimates of shape and scale parameters were obtained for both these and the central-tendency-type data.

SECTION VI

CONCLUSIONS AND RECOMMENDATIONS

1. CONCLUSIONS

This brief investigation has induced the following conclusions:

- a) The feasibility of using a large but simple specimen to obtain extrema data has been demonstrated.
- b) The ability to monitor the specimen sufficiently closely, to prevent initiated cracks from attaining a size such as to cause interference with adjacent details, was shown to be quite practical.
- c) Although the majority of the initiated cracks were at random locations, it is uncertain whether complete independence of all the initial cracked holes was obtained.
- d) A difference in fatigue performance at the drill-entry and drill-exit sides of the specimens was observed, with the majority of the initiated cracks occurring on the drill-exit side.
- e) Some discrepancy was noted between the finite element predictions of stress distribution over the panel and the observed strain gage measurements.
- f) The applicability of the reliability analysis procedure for predicting life to first failure in the panel, based on information from the single-hole specimens, has been substantiated.
- g) The Weibull model appears to better match the extrema fatigue data in this study.

2. RECOMMENDATIONS

Based on the above conclusions, the following recommendations can be made:

- a) Further analyses should be conducted to ascertain the cause of the discrepancy in the measured and predicted stress distributions across the panel.
- b) Further analyses of the fatigue results obtained from the large panels should be attempted. Corrections for differences in stress levels should be undertaken to normalize the data.
- c) Several panels should be tested to determine characteristic or median life at first failure.

NOT REPRODUCIBLE



Figure 1. Multihole Panel Mounted in the EMR 150,000-Lb Programmed Fatigue Testing Machine

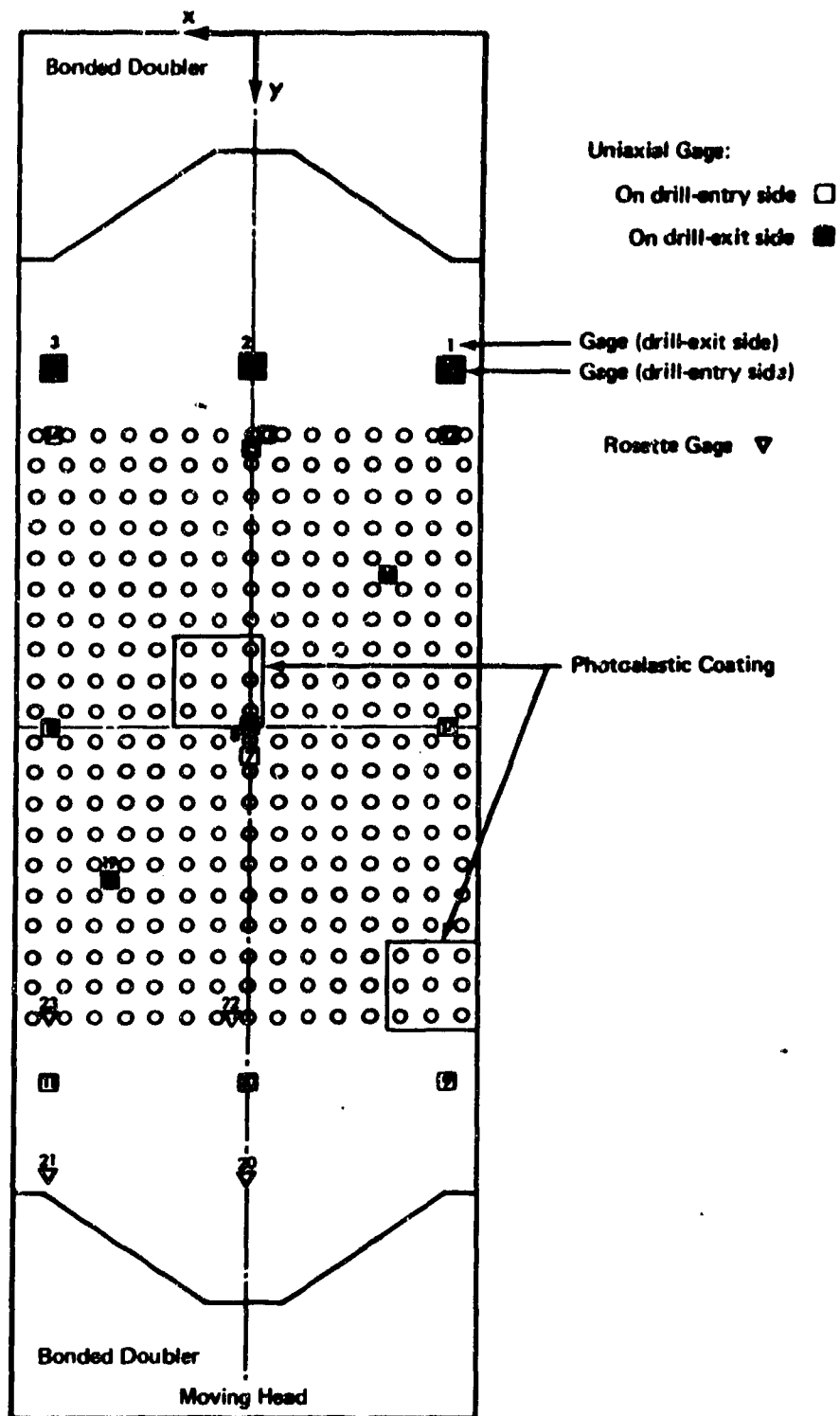


Figure 2. Panel 1—Location of Strain Gages and Photoelastic Coatings

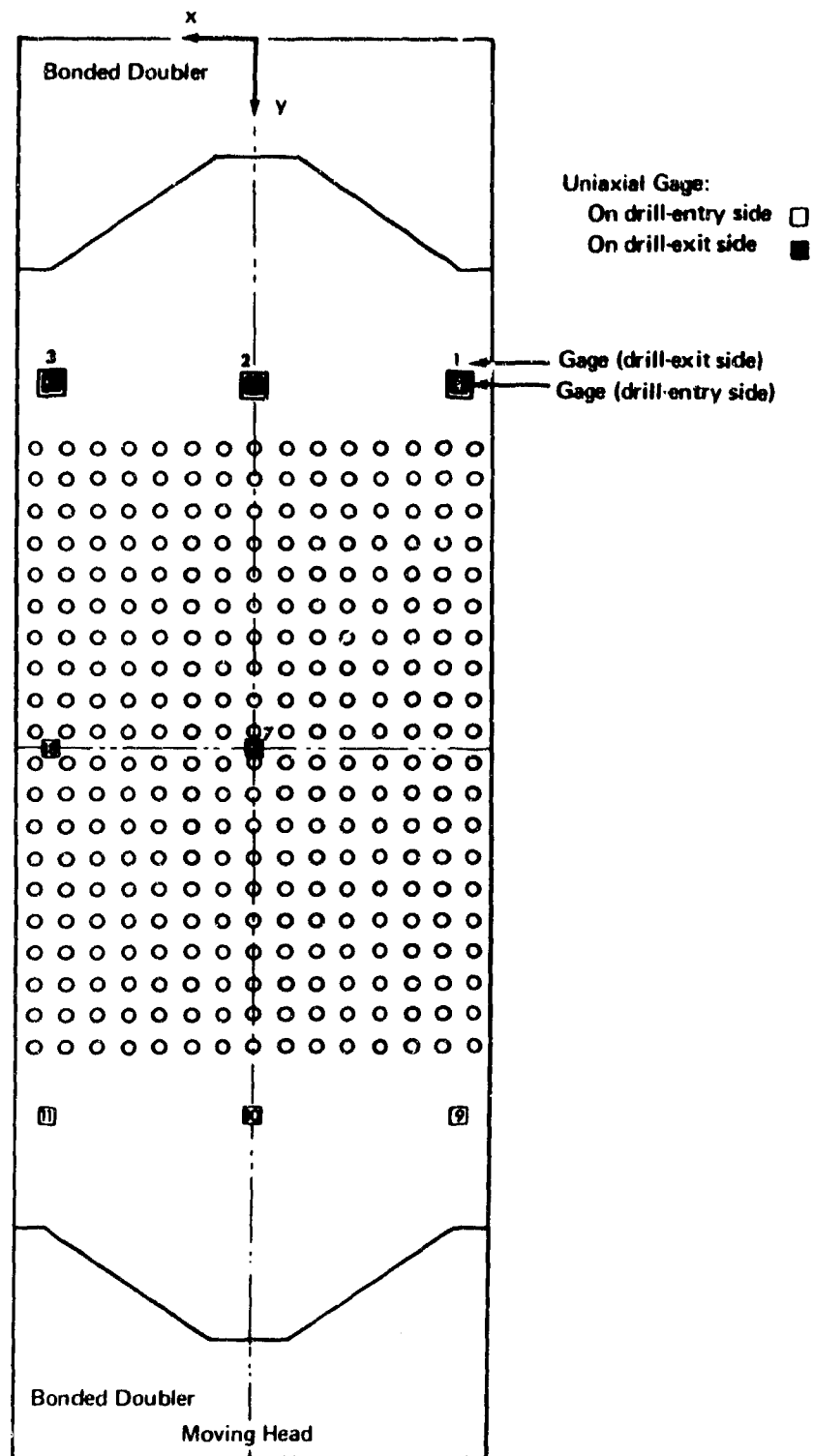


Figure 3. Panel 2—Location of Strain Gages

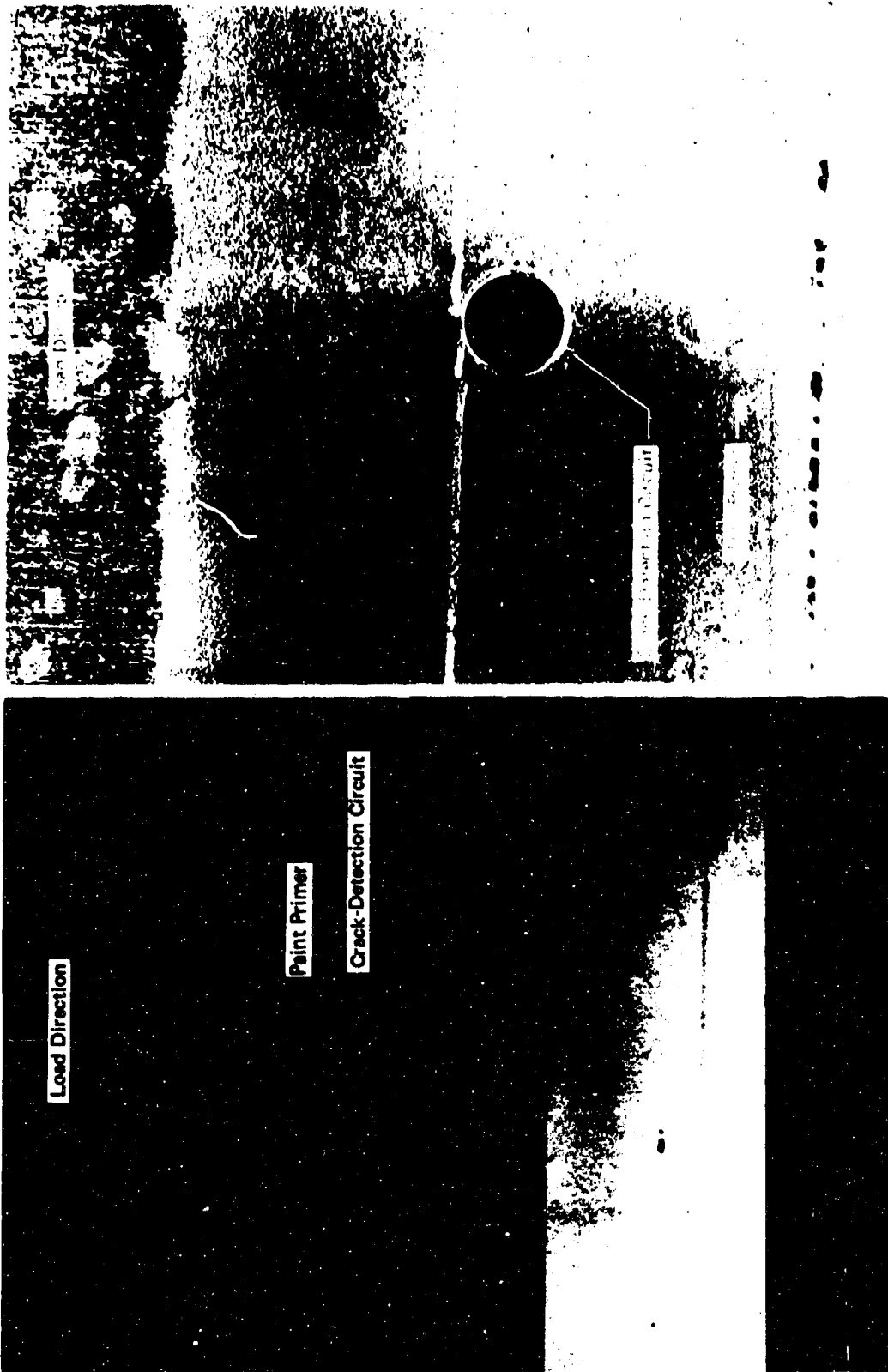


Figure 4. Typical Section Showing Crack-Detection Circuits

Figure 5. Detail of Crack-Detection Circuit Around a Single Hole

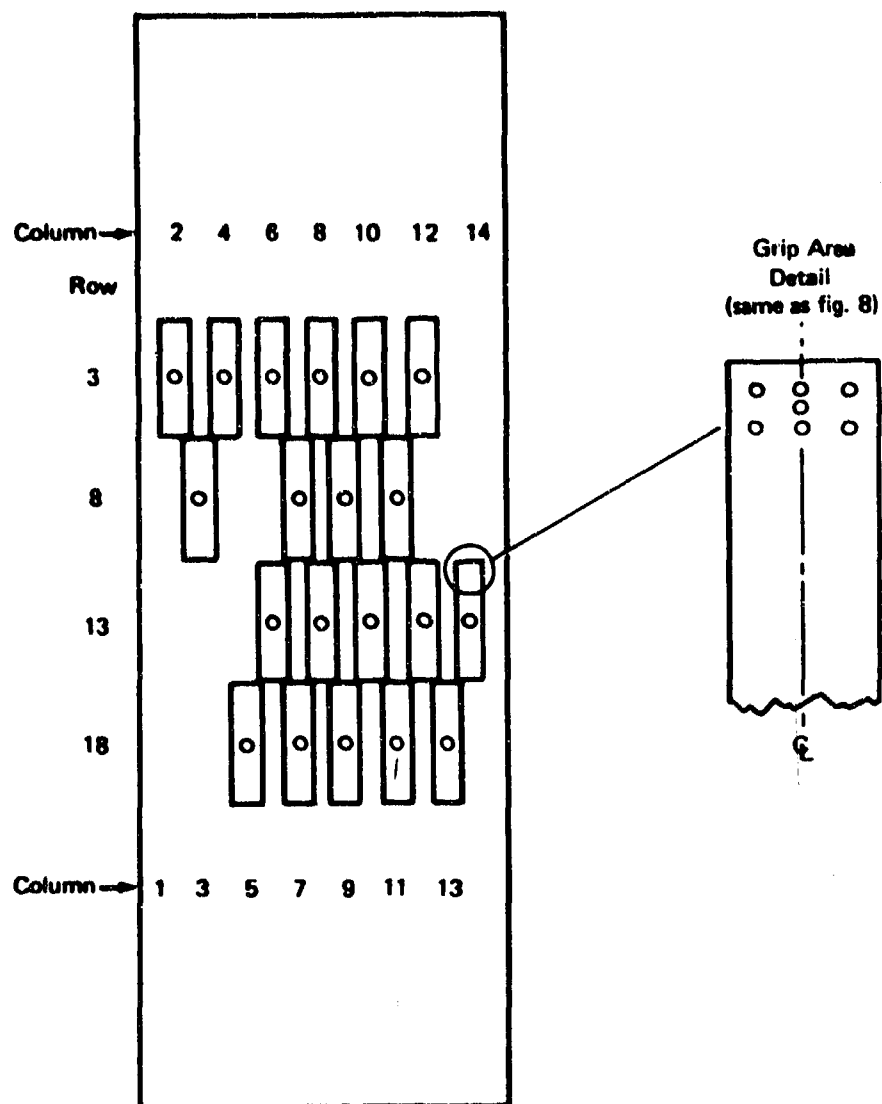


Figure 6. Location of Small Specimens Cut From Panel 3

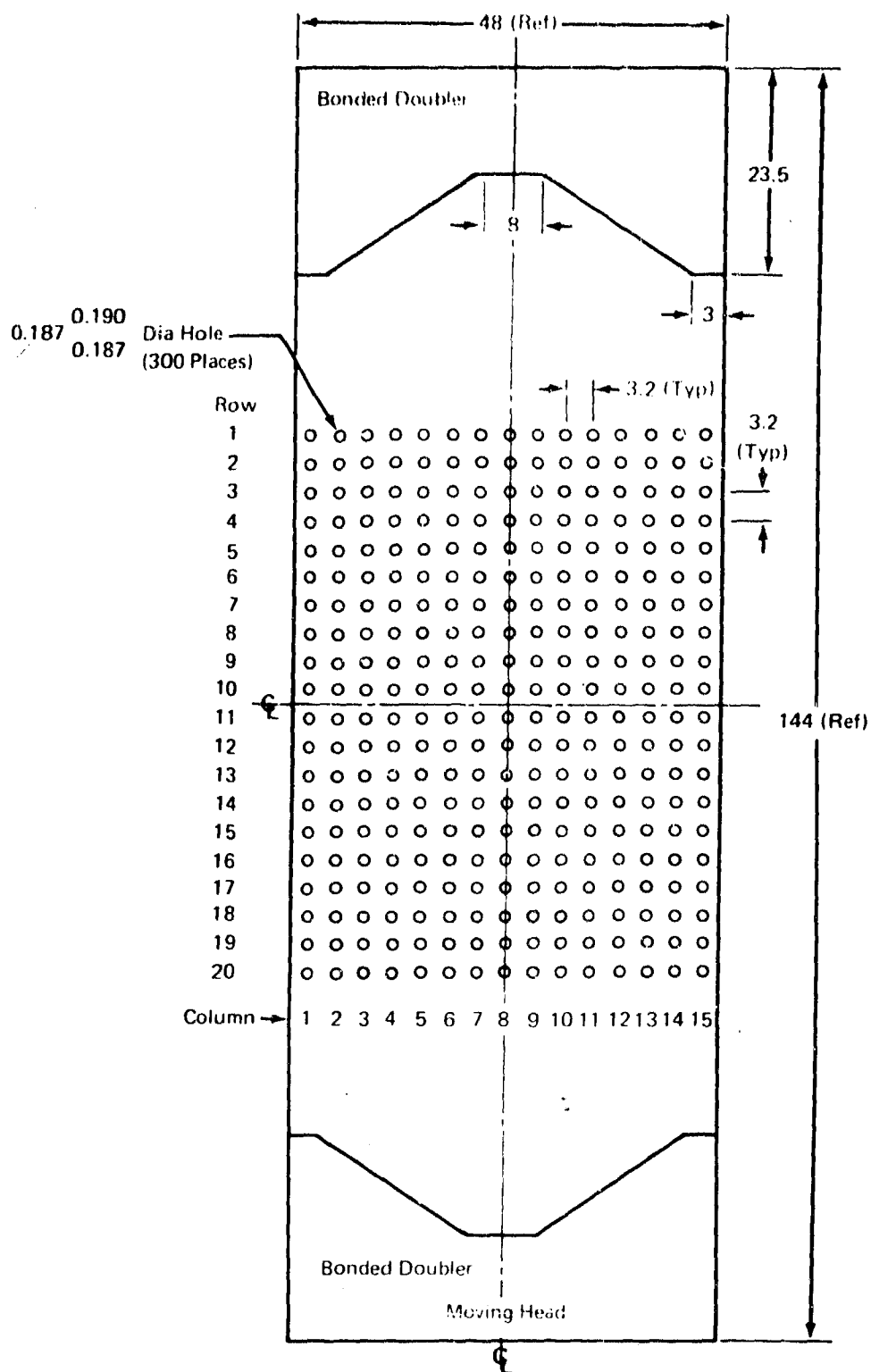


Figure 7. Multihole Panel

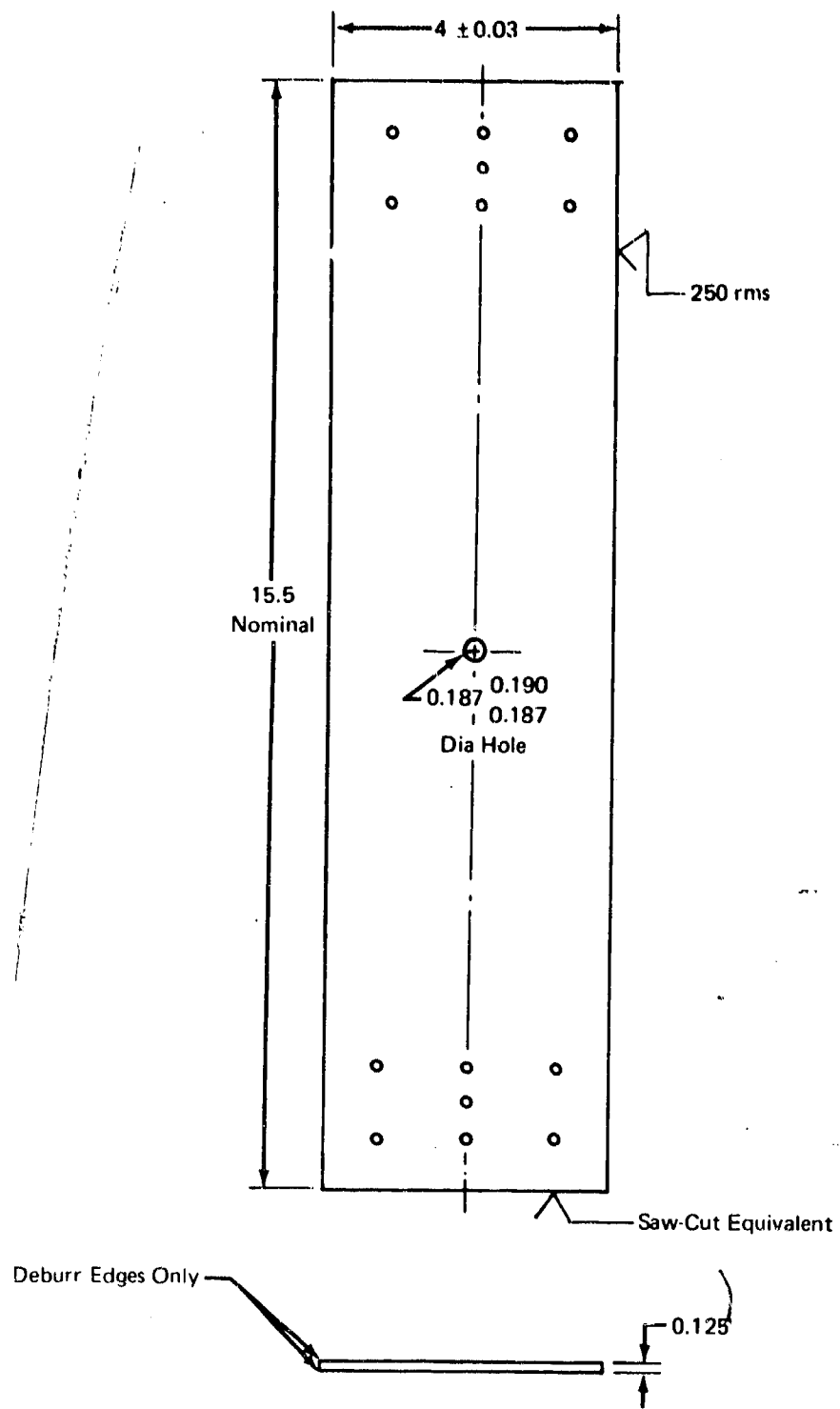


Figure 8. Single-Hole Specimen

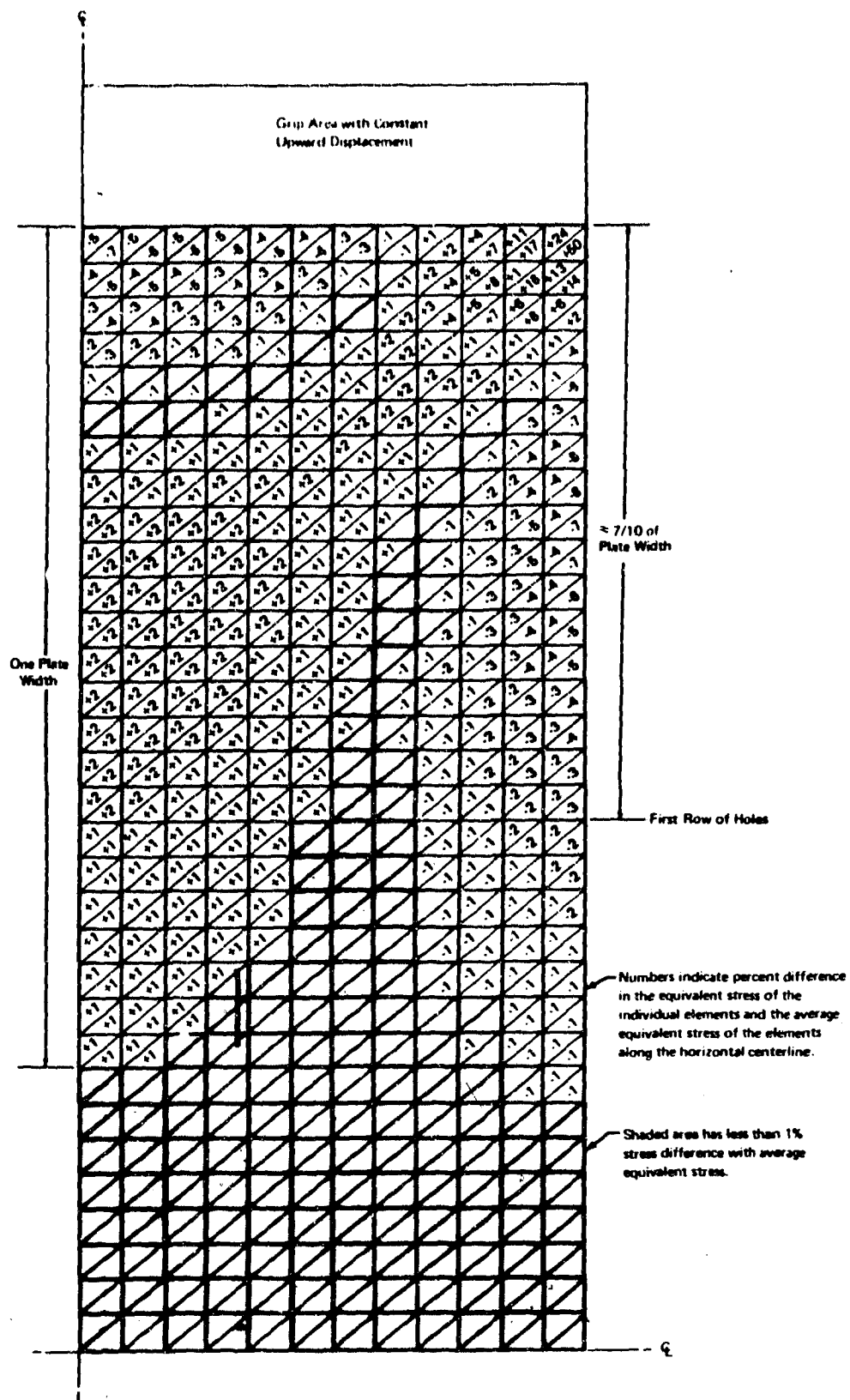


Figure 9. Computed Stress Variation for Panel With Constant Cross Section

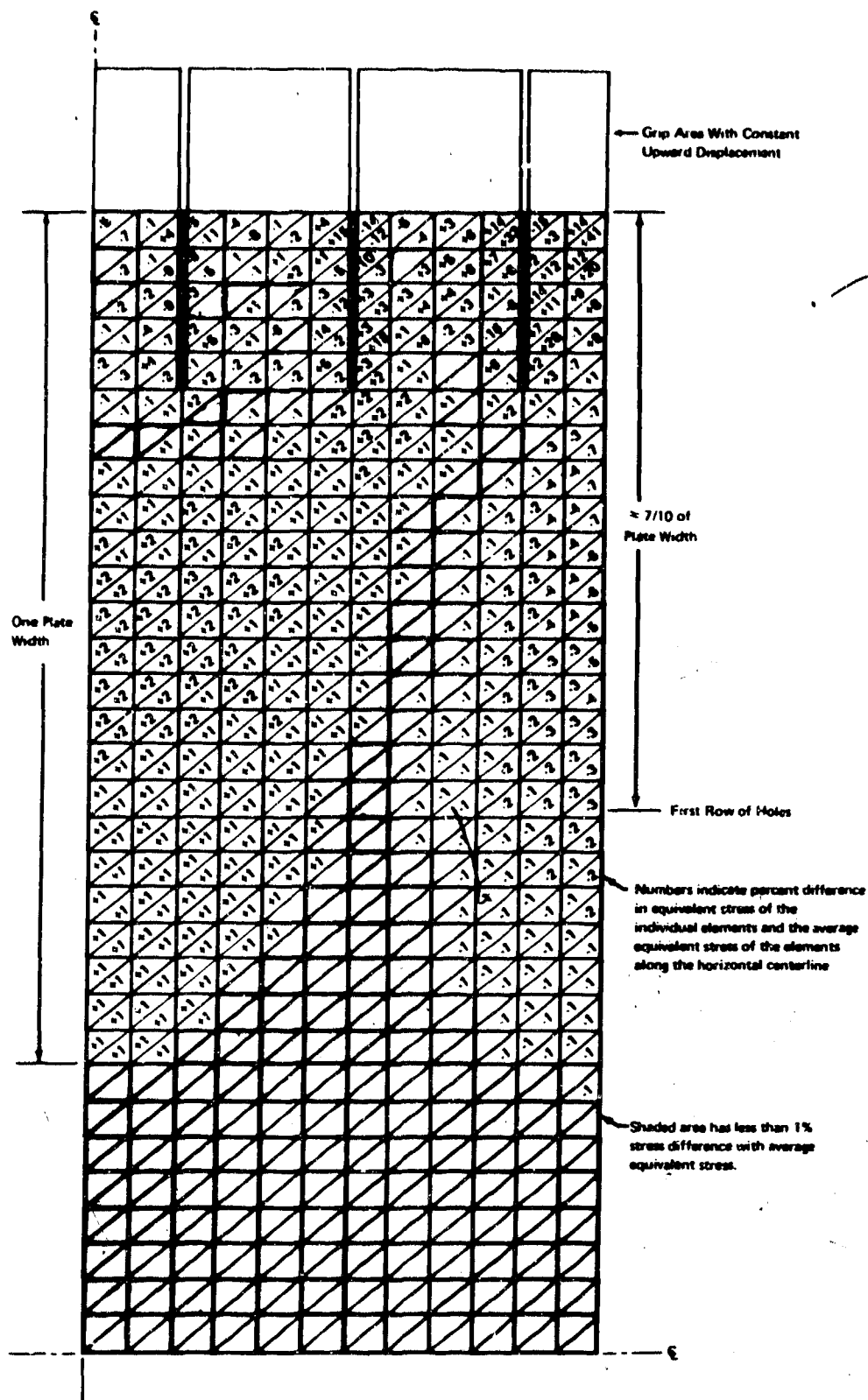


Figure 10. Computed Stress Variation for Panel With Slots in the Grip Area

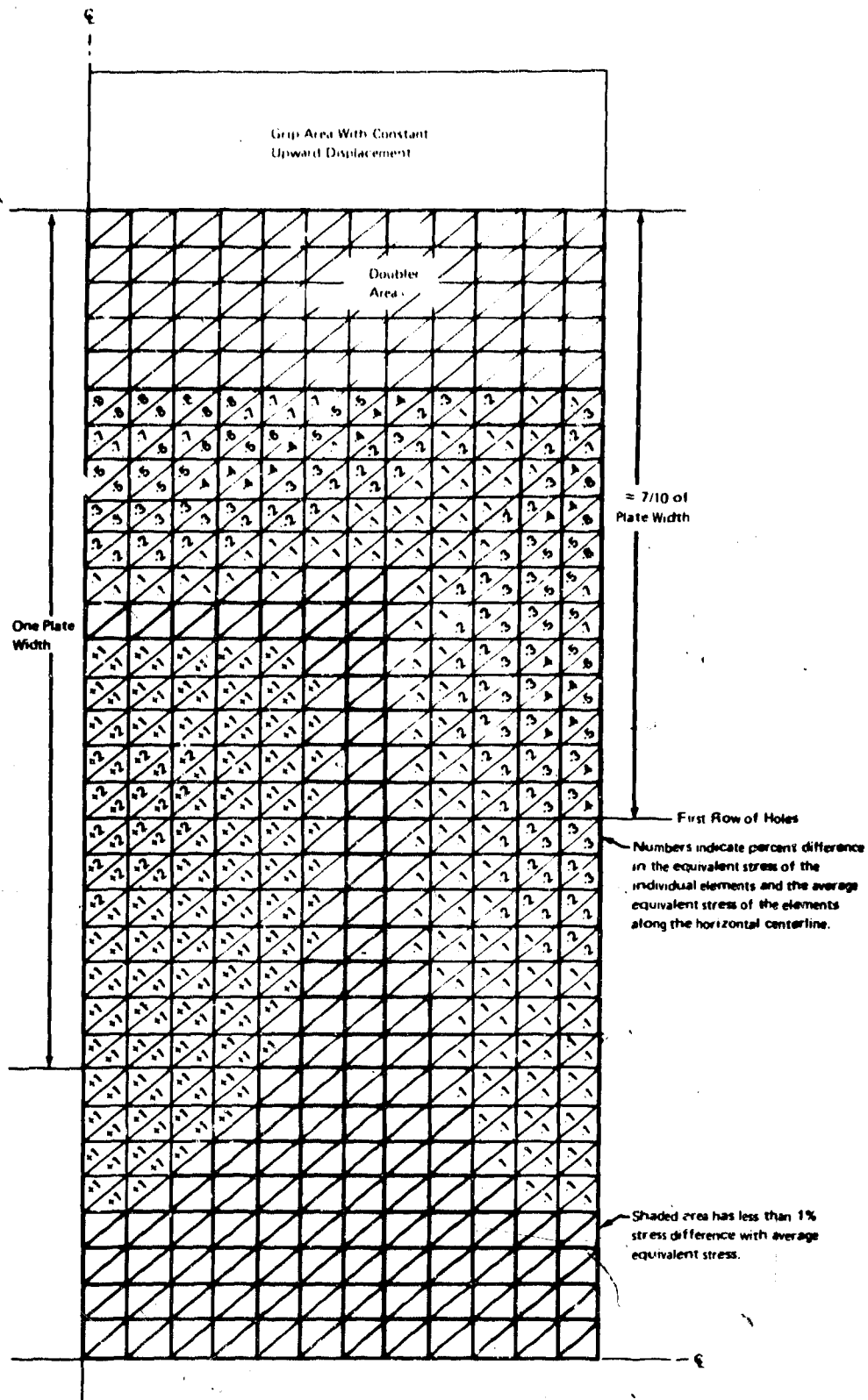


Figure 11. Computed Stress Variation for Panel With Rectangular Doublers

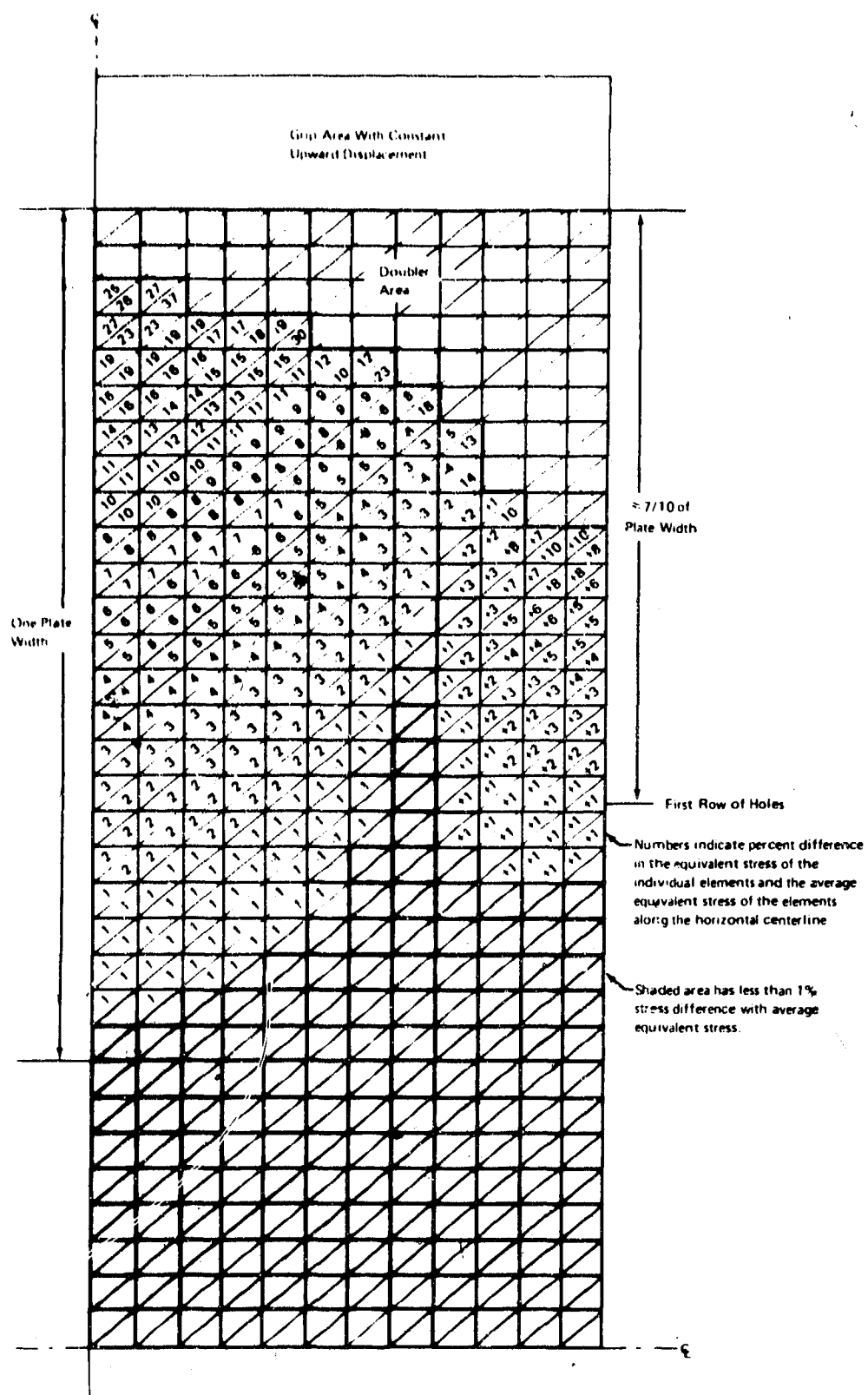


Figure 12. Computed Stress Variations for Panel With U-Shaped Doublers (Final Configuration)

NOT REPRODUCIBLE

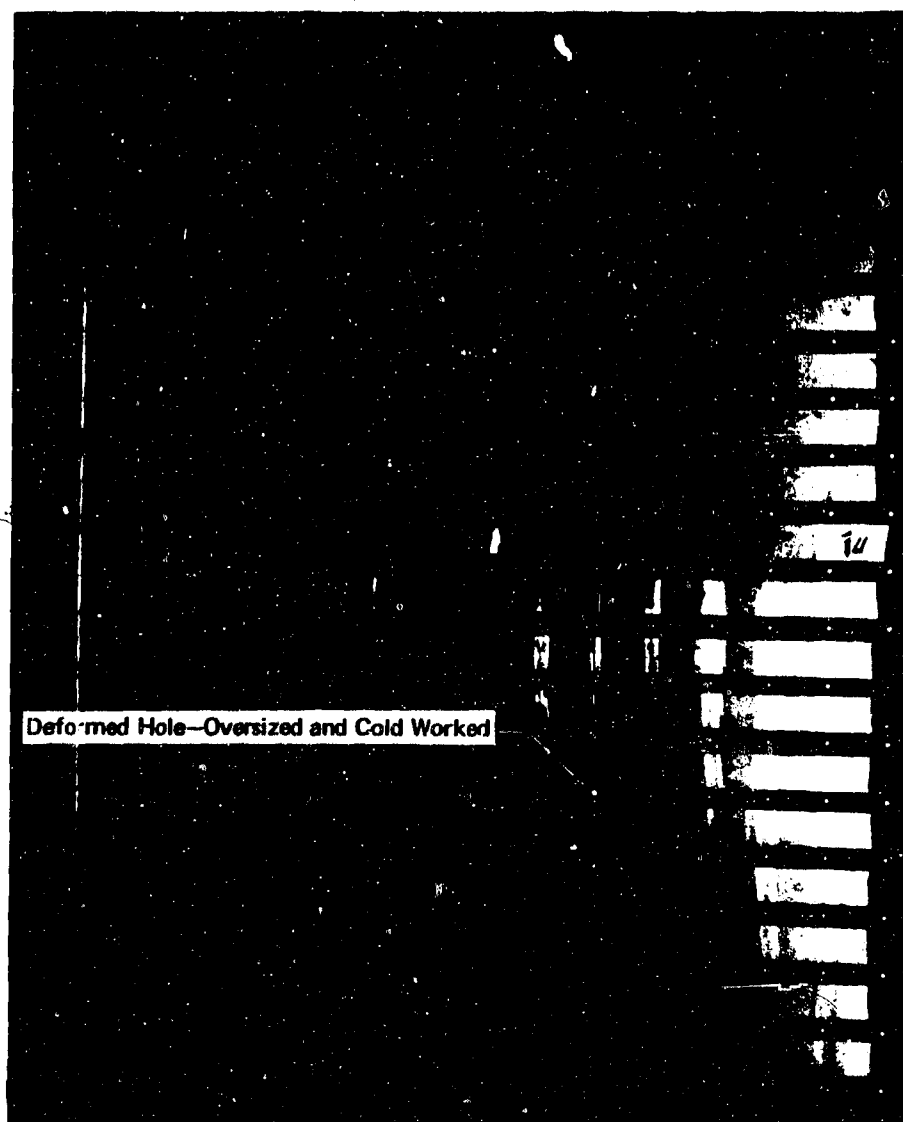


Figure 13. Panel 2—Hole Field

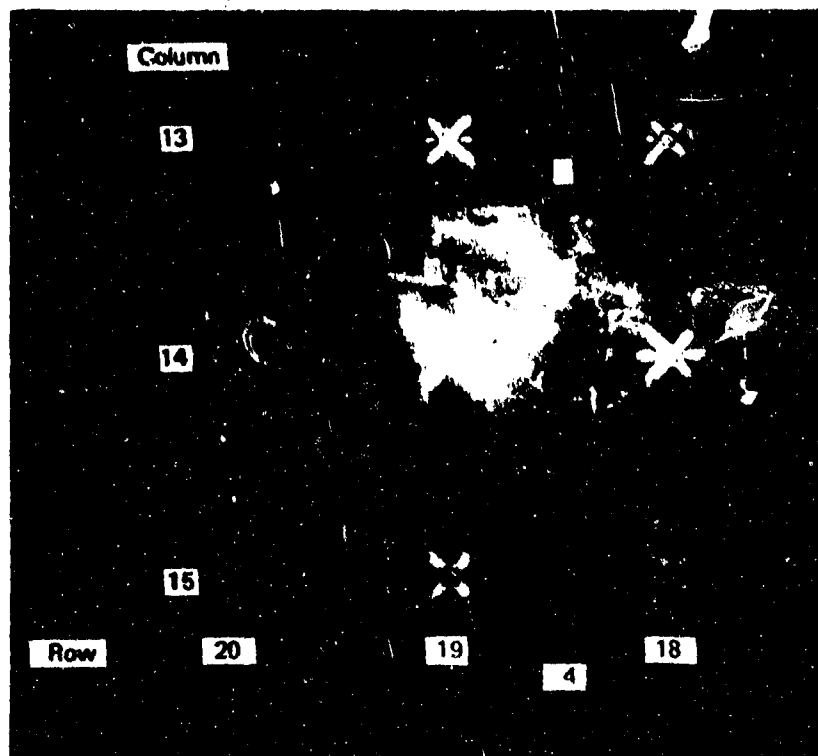


Figure 14. Photoelastic Coating at Lower Right of Panel 1



Figure 15. Photoelastic Coating at Central Portion of Panel 1

NOT REPRODUCIBLE

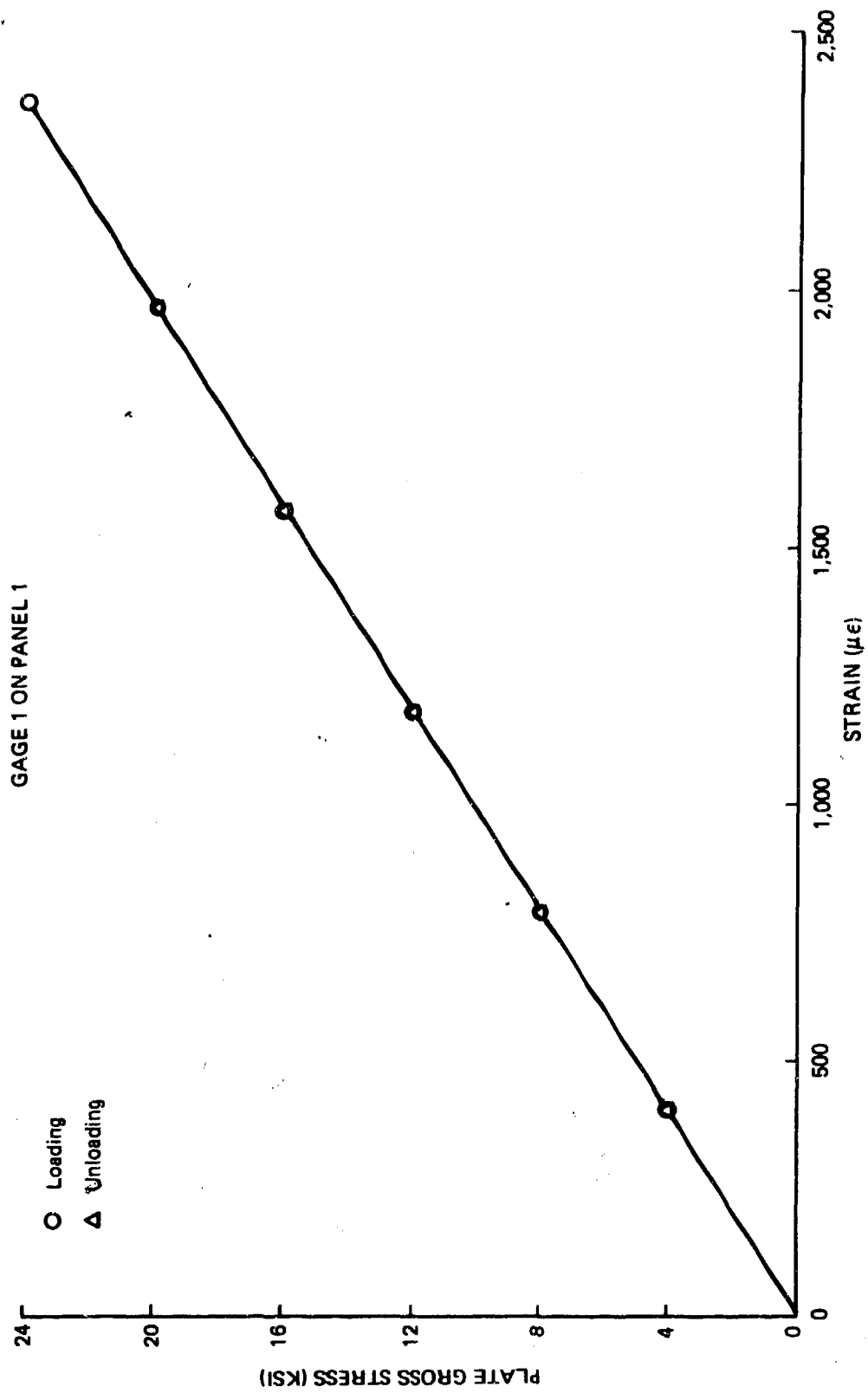


Figure 16. Typical Strain Gage Data During Loading and Unloading

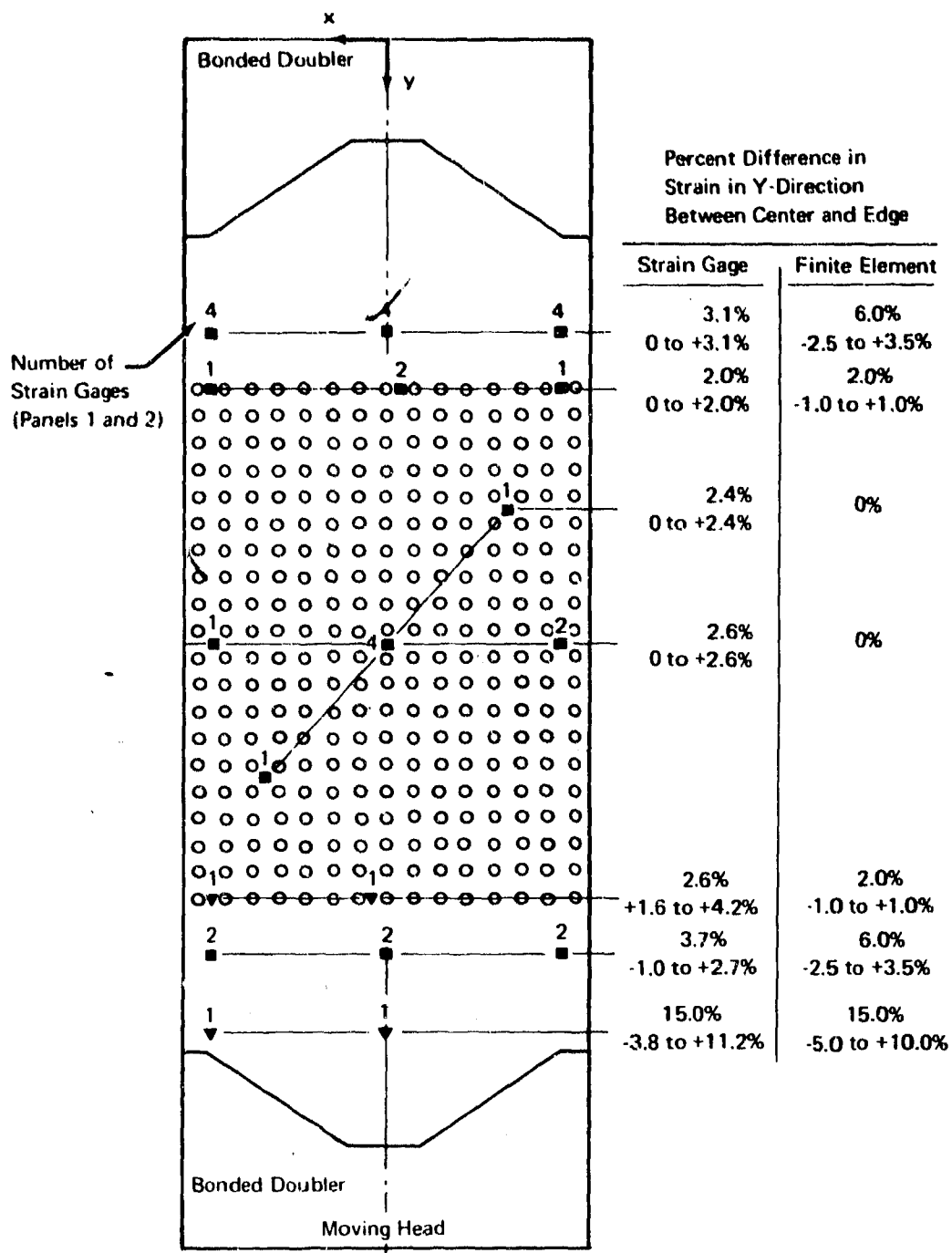


Figure 17. Percent Difference of Strain in Y-Direction Between Vertical Centerline and Edge of Panel

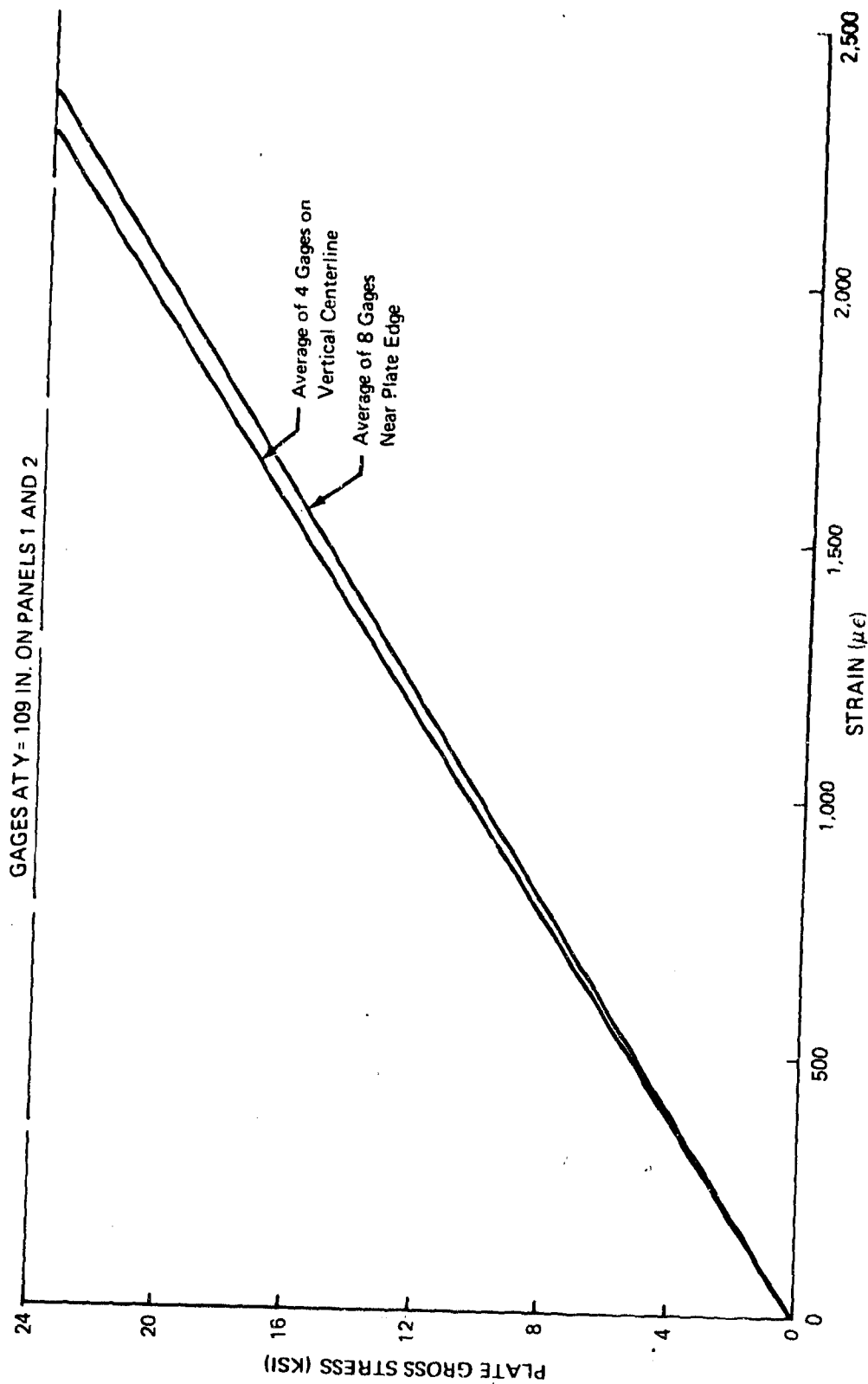


Figure 18. Difference in Strain Gage Readings Between Gages on the Vertical Centerline and Near the Panel Edge

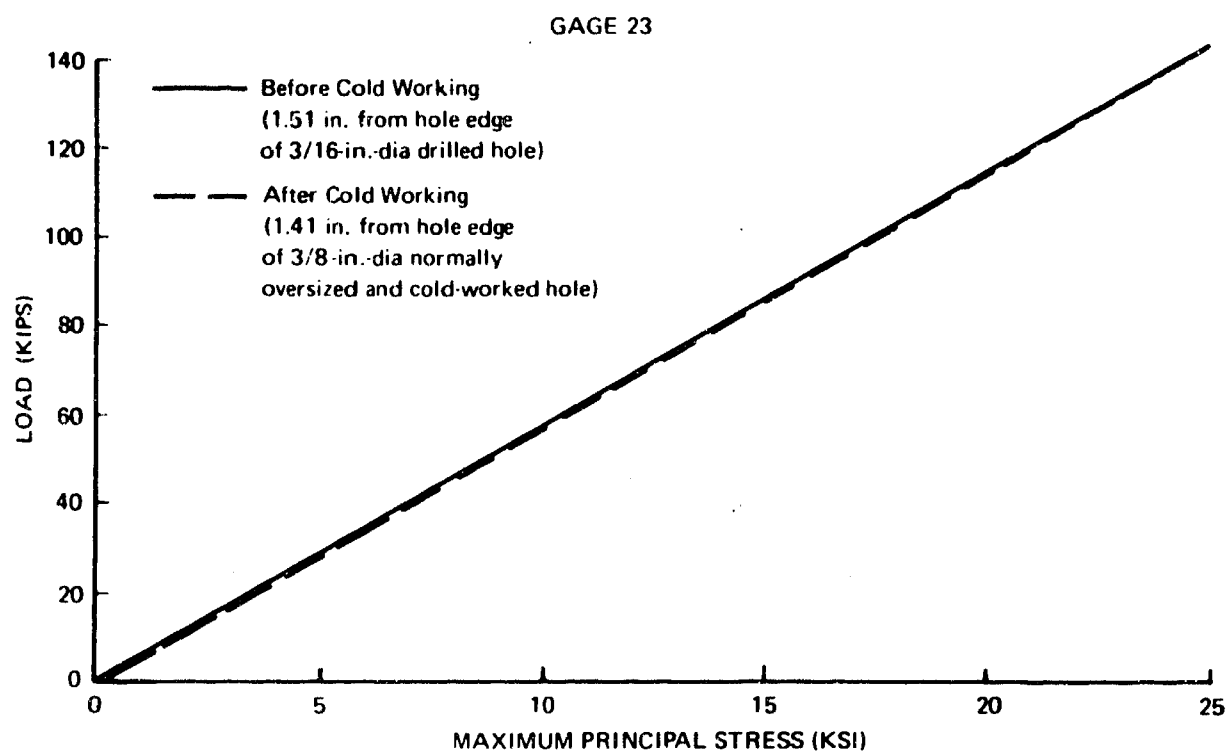
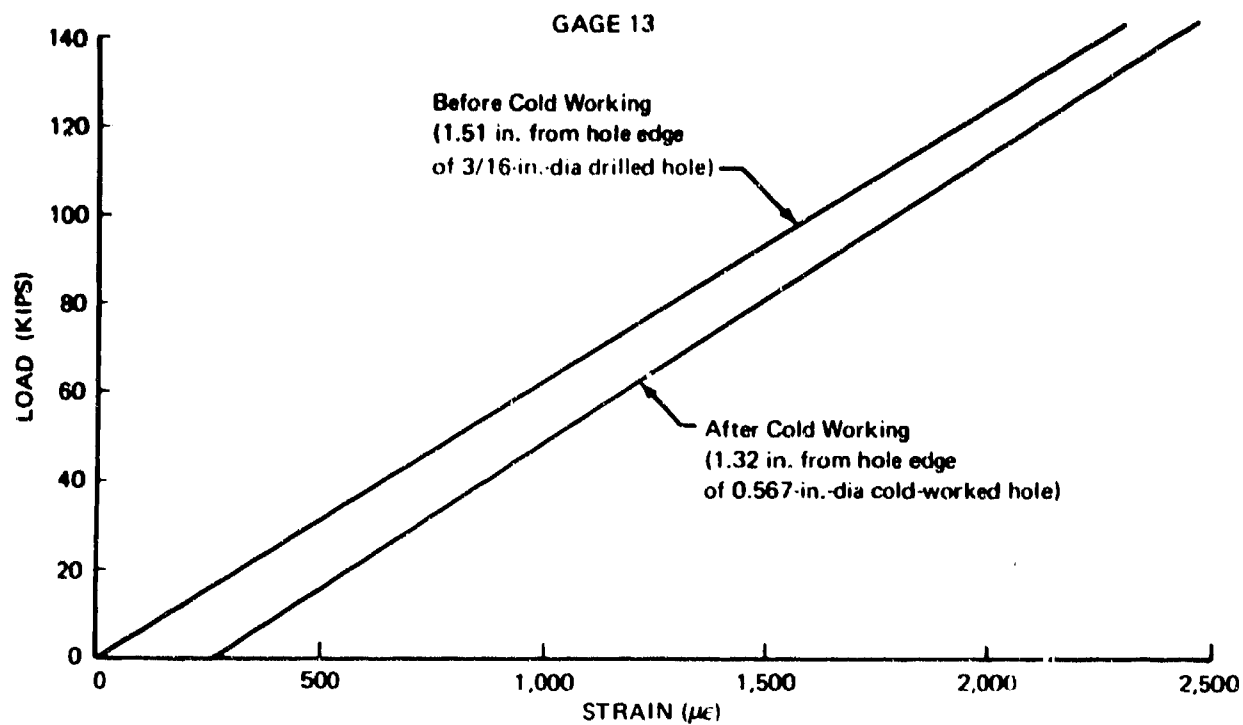


Figure 19. Strain Gage Data of Gages Next to Cold-Worked Holes

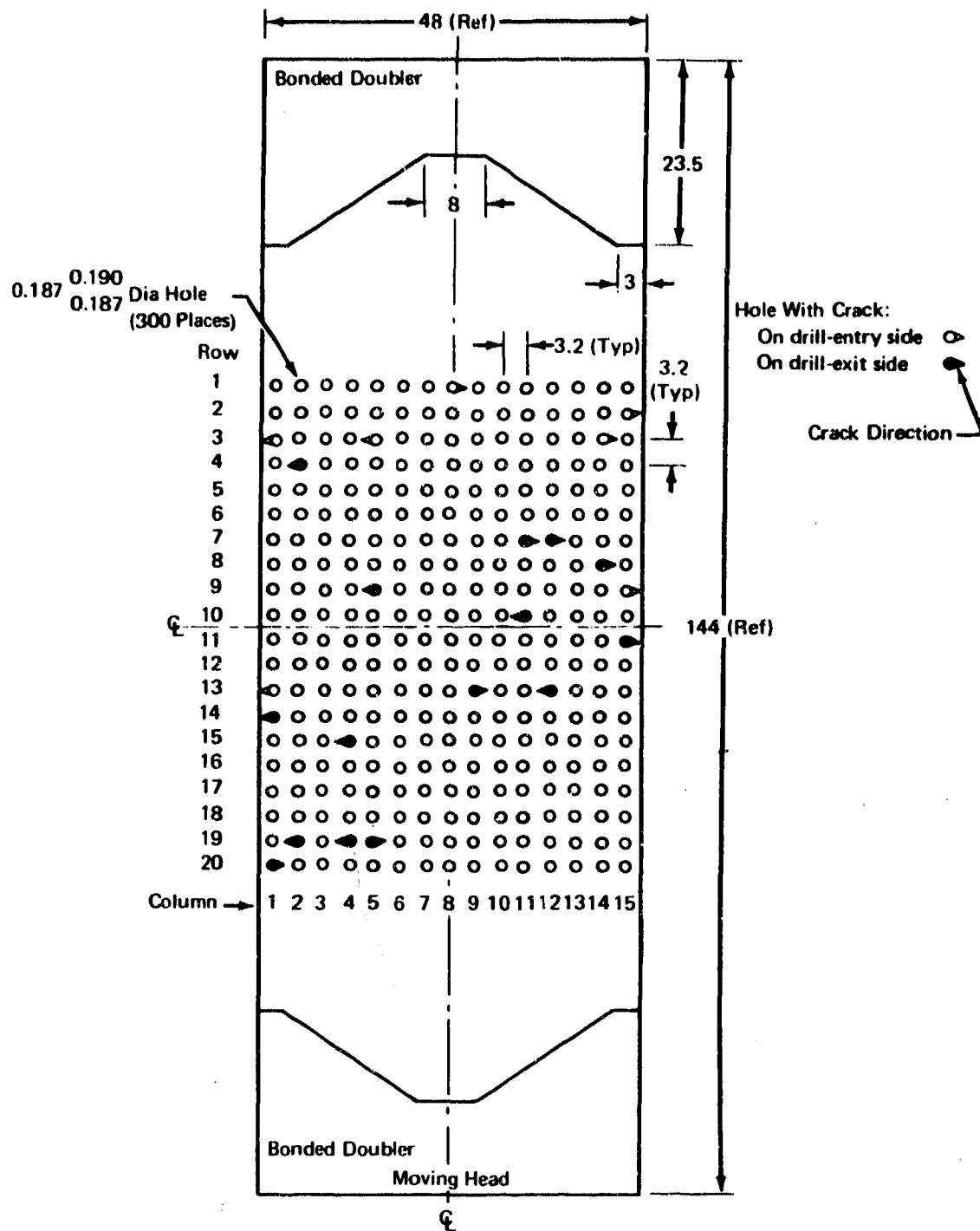


Figure 20. Location of Fatigue Cracks on Panel 1

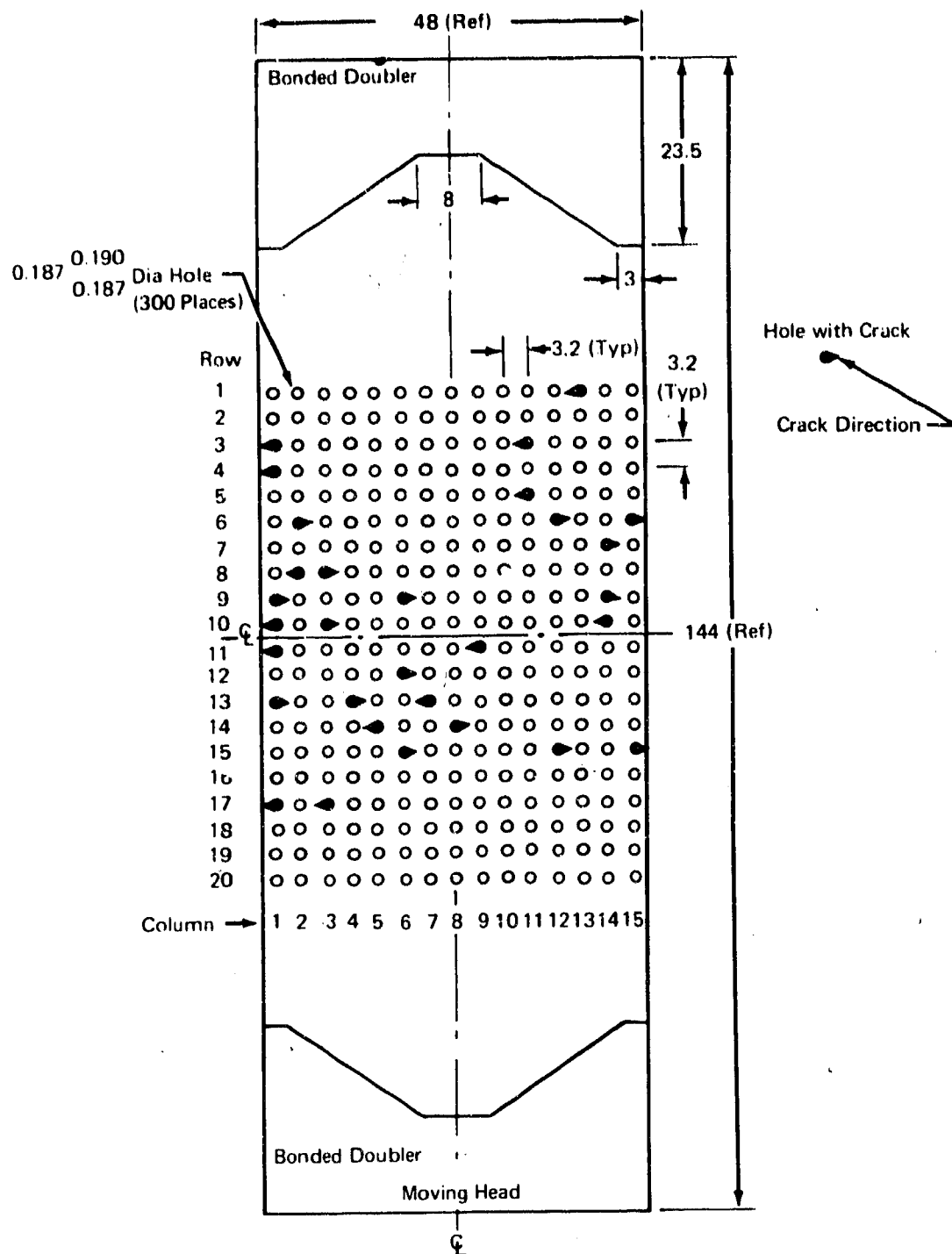
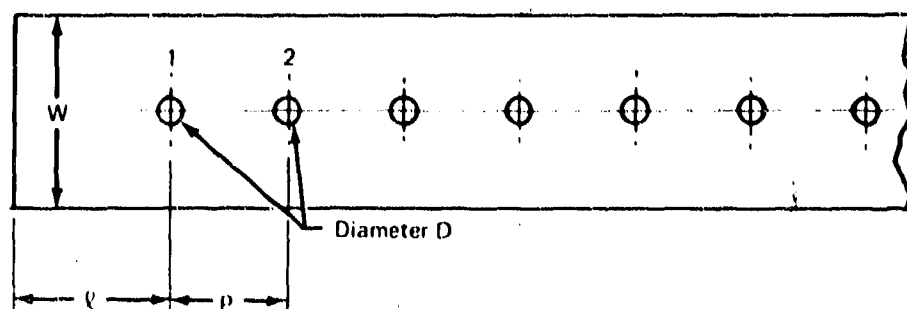


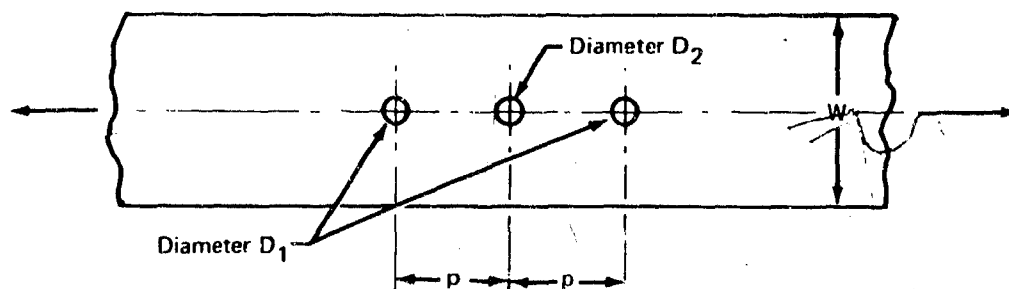
Figure 21. Location of Fatigue Cracks on Panel 2

Table 1. Results of a Finite Element Stress Analysis for a Strip of Aluminum Containing a Single Row of Holes Parallel to the Load Direction



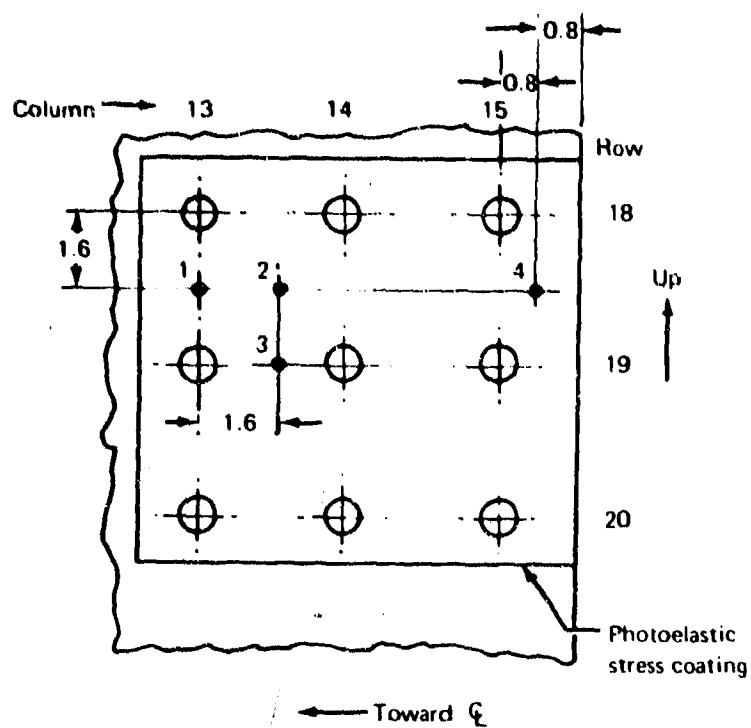
Case	$\frac{W}{D}$	$\frac{p}{D}$	$\frac{l}{D}$	K_{T1}	K_{T2}	$\frac{K_{T1}}{K_{T2}}$
1	10	6	5	3.15	3.08	1.023
2	10	5	5	3.13	3.03	1.033
3	10	4	5	3.09	2.96	1.044
4	10	6	9	3.11	3.08	1.010
5	10	5	9	3.09	3.03	1.020
6	10	4	9	3.05	2.95	1.034

Table 2. Results of a Photoelastic Stress Survey With a Single-Row, Three-Hole Model Loaded Parallel to the Row of Holes



Case	D_2	$\frac{W}{D_2}$	$\frac{p}{D_2}$	D_1	$\frac{W}{D_1}$	$\frac{p}{D_1}$	$\frac{D_1}{D_2}$	$\frac{K_{T1}}{K_{T2}}$
1	0.25	10.0	6.0	0.25	10.0	6.0	1.0	1.01
2	0.30	8.33	5.0	0.30	8.33	5.0	1.0	1.04
3	0.35	7.14	4.29	0.28	8.93	5.36	0.8	1.10
4	0.35	7.14	4.29	0.35	7.14	4.29	1.0	1.12
5	0.35	7.14	4.29	0.42	5.95	3.57	1.2	1.12
6	0.60	4.17	2.5	0.48	5.21	3.13	0.8	1.06
7	0.60	4.17	2.5	0.60	4.17	2.5	1.0	1.10
8	0.60	4.17	2.5	0.72	3.47	2.08	1.2	1.20

Table 3. Photoelastic Stress Data at Lower Right Location—Static Load of 144,000 Lb



Point	Thickness t_p (in.)	Calibration ($\mu\text{in./in./div}$)	R_c (div)	$\epsilon_1 - \epsilon_2$ ($\mu\text{in./in.}$)	$\sigma_1 - \sigma_2$ (ksi)
1	0.0678	20.65	149	3,077	24.5
2	0.0682	20.53	157	3,223	25.7
3	0.0681	20.56	155	3,187	25.4
4	0.0695	20.14	162	3,262	26.0

$$\sigma_1 - \sigma_2 = \frac{(\epsilon_1 - \epsilon_2)E}{1 + \mu}$$

where: $E = 10.6 \times 10^6$ psi
 $\mu = .33$

Table 4. Single-Hole Specimen Fatigue Test Results

Test	Hole location		Life to crack		Crack location		Life to failure (cycles)
	Row	Column	Crack length (in.)	Cycles	Drill entry or exit side	Hole side	
1	3	2	0.02	50,000	Exit	Left	71,000
2	13	8	0.02	43,000	Exit	Left	67,000
3	13	10	0.02	56,000	Entry	Left	74,000
4	8	3	0.02	50,000	Entry	Right	73,000
5	8	7	0.02	59,000	Entry	Right	73,000
6	8	9	0.02	45,000	Exit	Right	61,000
7	8	11	0.02	54,000	Exit	Right	76,000
8	18	13	0.02	42,000	Exit	Left	64,000
9	3	6	0.02	39,000	Exit	Left	58,000
10	3	8	0.02	46,000	Exit	Left	61,000
11	18	5	0.02	48,000	Exit	Left	67,000
12	13	14	0.02	46,000	Exit	Right	59,000
13	13	6	0.02	51,000	Exit	Left	68,000
14	3	10	0.02	40,000	Exit	Right	54,000
15	3	4	0.02	61,000	Entry	Right	72,000
16	13	12	0.02	41,000	Entry	Right	61,000
17	18	11	0.02	54,000	Entry	Left	67,000
18	18	7	0.02	37,000	Exit	Right	57,000
19	18	9	0.02	37,000	Exit	Left	58,000
20	3	12	0.02	55,000	Exit	Left	68,000

Table 5. Panel 1 Fatigue Test Results

Failure	Hole location		Life to crack		Crack location		Remarks
	Row	Column	Crack length (in.)	Cycles	Drill entry or exit side	Hole side	
1	2	15	0.02	18,768	Entry	Right	Hole with fabrication gouge
	15	4	0.02	19,504	Exit	Left	Hole with fabrication gouge
	3	14	0.06	20,500	Entry	Right	
2	10	11	0.02	20,576	Exit	Left	
3	14	1	0.02	20,604	Exit	Left	Hole with fabrication gouge
4	4	2	0.02	22,548	Exit	Left	
5	11	15	0.02	23,624	Exit	Right	
6	1	8	0.02	24,060	Entry	Right	Hole with fabrication gouge
7	8	14	0.02	24,390	Exit	Right	
8	7	11	0.02	24,690	Exit	Right	
9	9	5	0.02	26,060	Exit	Left	Adjacent to hole 14-1
10	13	1	0.02	26,400	Entry	Left	
11	19	5	0.02	26,760	Exit	Right	
12	19	2	0.04	26,780	Exit	Left	Adjacent to hole 4-2
13	3	1	0.03	26,901	Entry	Left	
14	9	15	0.02	26,901	Entry	Right	
15	1	8	0.06	26,901	Exit	Right	Adjacent to hole 8-14
	20	1	0.02	27,205			Reworked hole at 24,060
	13	12	0.05	27,385			Adjacent to hole 19-2
17	3	5	0.02	27,750	Entry	Left	Adjacent to hole 7-11
18	7	12	0.02	27,815	Exit	Right	
19	19	4	0.02	28,636	Exit	Left	
20	13	9	0.02	28,788	Exit	Right	Adjacent to hole 19-5

Table 6. Panel 2 Fatigue Test Results

Failure	Hole location		Life to crack		Crack location		Remarks
	Row	Column	Crack length (in.)	Cycles	Drill entry or exit side	Hole side	
1	8	3	0.02	28,615	Entry	Right	
2	15	6	0.02	29,498	Entry	Right	
3	12	6	0.03	34,850	Entry	Right	
4	4	1	0.02	35,688	Exit	Left	
5	10	1	0.02	36,160	Exit	Left	Adjacent to hole 10-1
6	9	1	0.02	36,228	Entry	Right	
7	10	3	0.02	36,320	Entry	Right	
8	1	13	0.02	36,480	Entry	Left	
9	9	6	0.02	36,555	Exit	Right	Adjacent to hole 10-1
10	11	1	0.02	36,572	Entry	Left	
11	15	12	0.02	36,597	Entry	Right	
12	10	14	0.02	37,035	Entry	Left	
13	14	8	0.02	37,246	Entry	Right	Adjacent to hole 15-6 Adjacent to hole 4-1
14	14	5	0.02	37,930	Exit	Left	
15	3	1	0.02	37,972	Entry	Left	
16	6	2	0.02	38,394	Exit	Right	
17	7	14	0.02	38,900	Entry	Right	Adjacent to hole 12-6
18	3	11	0.02	39,295	Entry	Left	
19	13	7	0.02	39,368	Entry	Left	
20	6	12	0.02	39,410	Entry	Right	
21	9	14	0.02	39,480	Entry	Right	Adjacent to hole 10-14 Adjacent to hole 6-12
22	5	11	0.02	39,518	Exit	Left	
23	17	3	0.02	39,610	Exit	Left	
24	15	15	0.02	39,626	Entry	Right	
25	6	15	0.02	39,658	Entry	Right	Adjacent to hole 7-14 Adjacent to hole 14-5
26	13	4	0.02	39,996	Entry	Right	
27	17	1	0.02	40,152	Exit	Left	
28	11	9	0.02	40,212	Exit	Left	
29	13	1	0.02	40,333	Entry	Right	Adjacent to hole 8-3
30	8	2	0.02	40,423	Entry	Left	

Table 7. Statistical Parameters of Single-Hole Specimen Data

Failure order	Hole location		Life to 0.02-in. long crack (cycles)	Weibull		Log-Normal		Remarks
	Row	Column		Scale parameter (cycles)	Shape parameter	Scale parameter (cycles)	Shape parameter	
Drill-exit side								
1	18	7	37,000	53,250	5.55	49,100	0.082	Censored sample, 14 failures (20 tested)
2	18	9	37,000					
3	3	6	39,000					
4	3	10	40,000					
5	18	13	42,000					
6	13	8	43,000					
7	8	9	45,000					
8	13	14	46,000					
9	3	8	46,000					
10	18	5	48,000					
11	3	2	50,000					
12	13	6	51,000					
13	8	11	54,000					
14	3	12	55,000					
Drill-entry side								
1	13	12	41,000	56,900	10.85	54,000	0.051	Censored sample, 6 failures (20 tested)
2	8	3	50,000					
3	18	11	54,000					
4	13	10	56,000					
5	8	7	59,000					
6	3	4	61,000					

Table 8. Comparison of Predicted Time to First Failure in 300 Details and the Multihole Panel Test Results

Description	Weibull distribution (eq. V-26)*	Log-normal distribution (eq. V-28)*	Panel 1 first failure	Panel 2 first failure
Total specimens	20	20		
Drill-entry side	6	6		
Failures in censored sample	10.85	0.051		
Shape parameter	56,900	54,000		
Scale parameter (cycles)				
0.95 lower bound of scale parameter (cycles)	54,100	49,000		
Drill-exit side	14	14		
Failures in censored sample	5.55	0.082		
Shape parameter	53,250	49,100		
Scale parameter (cycles)				
0.95 lower bound of scale parameter (cycles)	49,400	44,900		
Predicted time to first failure of 300 equal and independent details assuming a median level of reliability of the weakest	30,900	35,200	24,060	28,615
Drill-entry side				
Drill-exit side	16,500	26,400	19,504	...
Average life	48,000	48,000		
Shape parameter	4.0	0.14		
0.95 lower bound of scale parameter (cycles)	36,400	28,200		
Predicted time to first failure in 300 assuming a median level of reliability of the weakest	8,000	11,200		

$$\bar{Y}_R = \bar{Z} \bar{R} = 3 \left[\left(\frac{2n_f}{N} \right) \left(\frac{R_{n(1/R)}}{X^2_{\gamma}(2n_f)} \right) \right]^{1/\alpha}$$

(eq. V-26 from ref. 1)

$$\bar{Y}_R = 10 \left[\mu + k_R \sigma \right] = 10 \left[\hat{\mu} + \left(\frac{k_R}{\sqrt{\pi}} + k_R \right) \sigma \right]$$

(eq. V-28 from ref. 1)

*From ref. 1

Table 9. Comparison of Distribution Parameters Obtained From the Single-Hole and Multihole Test Specimens

Description			Single-hole specimens	Multihole specimens	
				Panel 1	Panel 2
Total specimens			20	297	299
Failures in censored sample used for estimate	Drill-entry side		6	...	20
	Drill-exit side		14	12	...
Weibull distribution (eqs. IV-15 and IV-16)	Shape parameter	Drill entry side	10.85		10.1
		Drill-exit side	5.55	5.26	
	Scale parameter (cycles)	Drill-entry side	56,900		52,000
		Drill-exit side	53,250	50,200	
	0.95 lower bound on scale parameter (cycles)	Drill entry side	54,100		50,200
		Drill-exit side	49,400	46,300	
Log-normal distribution (eq. IV-21)	Shape parameter	Drill-entry side	0.051		0.098
		Drill-exit side	0.082	0.181	
	Scale parameter (cycles)	Drill-entry side	54,000		57,000
		Drill-exit side	49,100	59,500	
	0.95 lower bound on scale parameter (cycles)	Drill-entry side	49,000		52,200
		Drill exit side	44,900	47,900	

$$\frac{\sum_{i=1}^{n_f} x_i^{1/\hat{k}} \ln x_i + \sum_{i=1}^{n_g} G_i^{1/\hat{k}} \ln G_i}{\sum_{i=1}^{n_f} x_i^{1/\hat{k}} + \sum_{i=1}^{n_g} G_i^{1/\hat{k}}} - \hat{k} = \frac{1}{n_f} \sum_{i=1}^{n_f} \ln x_i \quad (\text{eq. IV-15 from ref. 1})$$

$$\hat{\beta} = \left[\frac{1}{n_f} \left(\sum_{i=1}^{n_f} x_i^{1/\hat{k}} + \sum_{i=1}^{n_g} G_i^{1/\hat{k}} \right) \right]^{\hat{k}} \quad (\text{eq. IV-16 from ref. 1})$$

$$\left. \begin{aligned} s^2 &= \hat{\sigma}^2 \left[1 - \frac{1}{n_f} \sum_{i=1}^{n_g} \epsilon_i h_i - \left(\frac{1}{n_f} \sum_{i=1}^{n_g} h_i \right)^2 \right] \\ \bar{x}_L &= \hat{\mu} - \frac{1}{n_f} \sum_{i=1}^{n_g} h_i \end{aligned} \right\} \quad (\text{eq. IV-21 from ref. 1})$$

APPENDIX

STATIC STRAIN SURVEY DATA

This appendix comprises tables of data relating to the two multihole panels. Tables are presented establishing the location coordinates of the axial and rosette strain gages on panel 1 and the strain gages on panel 2. The strain readouts from all the static loadings for both panels are tabulated, and the reduced rosette data are also included.

Strain Gage Locations on Panel 1

Gage	Location				Type	
	x (in.)	y (in.)	Drill entry side	Drill exit side	Uniaxial	Rosette
1	-21	35	●		●	
2	0	35	●		●	
3	+21	35	●		●	
4	-21	35		●	●	
5	0	35		●	●	
6	+21	35		●	●	
7	0	75.2	●		●	
8	0	72		●	●	
9	-21	109	●		●	
10	0	109	●		●	
11	+21	109	●		●	
12	-20.8	41.6	●		●	
13	- 1.6	41.6	●		●	
14	+20.8	41.6	●		●	
15	0	43.2	●		●	
16	-14.4	56	●		●	
17	-20.8	72	●		●	
18	+20.8	72	●		●	
19	+14.4	88		●	●	
20	0	120	●			●
21	+21	120	●			●
22	+ 1.6	102.4	●			●
23	+20.8	102.4	●			●

Strain Gage Data, Panel 1, First Cycle Before Fatigue Test

INCREASING LOAD

Gage	Load (lb)	Strain ($\mu\epsilon$)					
	0	24,000	48,000	72,000	96,000	120,000	144,000
1		415	807	1,202	1,594	1,983	2,381
2		421	800	1,183	1,597	1,944	2,330
3		415	800	1,192	1,568	1,973	2,368
4		382	774	1,166	1,558	1,947	2,343
5		314	690	1,069	1,448	1,824	2,208
6		350	735	1,131	1,520	1,912	2,307
7		295	674	1,056	1,432	1,811	2,193
8		424	784	1,153	1,523	1,889	2,265
9		431	820	1,212	1,607	1,999	2,394
10		421	797	1,176	1,555	1,931	2,313
11		402	791	1,186	1,578	1,973	2,368
12		437	826	1,218	1,607	1,996	2,388
13		411	794	1,179	1,558	1,941	2,330
14		408	794	1,183	1,571	1,957	2,349
15		405	784	1,163	1,542	1,921	2,304
16		376	765	1,153	1,542	1,931	2,326
17		353	745	1,134	1,529	1,918	2,313
18		356	752	1,147	1,536	1,925	2,317
19		444	833	1,225	1,610	1,999	2,394

DECREASING LOAD

Gage	Load (lb)	Strain ($\mu\epsilon$)				
	120,000	96,000	72,000	48,000	24,000	0
1	1,986	1,597	1,209	813	428	
2	1,947	1,568	1,186	807	424	
3	1,976	1,588	1,199	810	421	
4	1,950	1,558	1,170	778	389	
5	1,827	1,452	1,072	693	318	
6	1,915	1,526	1,134	745	356	
7	1,814	1,435	1,059	677	298	
8	1,895	1,526	1,160	794	434	
9	1,999	1,607	1,215	823	434	
10	1,938	1,558	1,183	804	424	
11	1,973	1,581	1,189	794	408	
12	1,999	1,610	1,221	833	444	
13	1,944	1,562	1,179	794	418	
14	1,960	1,575	1,186	800	418	
15	1,925	1,542	1,166	784	408	
16	1,934	1,545	1,153	768	382	
17	1,921	1,533	1,140	748	356	
18	1,928	1,539	1,147	758	363	
19	2,002	1,617	1,225	836	447	

Strain Gage Data, Panel 1, Second Cycle Before Fatigue Test

INCREASING LOAD

Gage \ Load (lb)	Strain (μϵ)						
	0	24,000	48,000	72,000	96,000	120,000	144,000
1		399	791	1,176	1,563	1,963	2,362
2		402	781	1,160	1,535	1,925	2,310
3		386	771	1,157	1,549	1,941	2,339
4		366	758	1,144	1,533	1,928	2,323
5		298	674	1,050	1,432	1,811	2,193
6		324	713	1,102	1,494	1,809	2,281
7		282	661	1,037	1,419	1,795	2,177
8		402	785	1,128	1,497	1,869	2,239
9		411	804	1,192	1,588	1,986	2,375
10		405	778	1,157	1,536	1,921	2,297
11		379	768	1,157	1,555	1,957	2,349
12		411	800	1,189	1,581	1,976	2,359
13		395	774	1,157	1,539	1,928	2,304
14		382	765	1,150	1,536	1,931	2,317
15		386	761	1,137	1,520	1,905	2,281
16		360	745	1,131	1,523	1,921	2,304
17		330	723	1,118	1,507	1,905	2,291
18		327	719	1,115	1,507	1,902	2,287
19		424	813	1,199	1,594	1,989	2,372

DECREASING LOAD

DECREASING LOAD						
Load (lb)	Strain ($\mu\epsilon$)					
Gage	120,000	96,000	72,000	48,000	24,000	0
1	1,963	1,568	1,182	794	405	
2	1,921	1,539	1,163	784	405	
3	1,941	1,545	1,163	778	392	
4	1,928	1,536	1,150	761	369	
5	1,808	1,429	1,053	680	301	
6	1,886	1,494	1,108	719	330	
7	1,788	1,409	1,037	661	285	
8	1,866	1,497	1,137	771	408	
9	1,973	1,581	1,196	807	415	
10	1,915	1,536	1,163	784	411	
11	1,947	1,552	1,166	774	386	
12	1,967	1,575	1,192	807	418	
13	1,918	1,533	1,157	781	399	
14	1,924	1,536	1,153	768	386	
15	1,895	1,513	1,140	765	392	
16	1,908	1,516	1,134	748	363	
17	1,895	1,503	1,118	729	337	
18	1,892	1,500	1,118	729	369	
19	1,980	1,588	1,205	820	431	

Strain Gage Data, Panel 1, Third Cycle Before Fatigue Test

INCREASING LOAD							
Gage	Load (lb)	Strain ($\mu\epsilon$)					
	0	24,000	48,000	72,000	96,000	120,000	144,000
1		405	794	1,183	1,575	1,970	2,365
2		405	784	1,166	1,545	1,928	2,313
3		395	778	1,166	1,558	1,947	2,346
4		373	761	1,150	1,542	1,931	2,330
5		305	680	1,056	1,435	1,811	2,197
6		334	719	1,108	1,500	1,892	2,284
7		285	664	1,043	1,422	1,801	2,184
8		411	771	1,134	1,503	1,869	2,242
9		421	810	1,202	1,594	1,989	2,385
10		285	784	1,160	1,542	1,918	2,304
11		392	778	1,170	1,565	1,960	2,355
12		418	807	1,196	1,588	1,976	2,368
13		399	781	1,163	1,545	1,928	2,313
14		389	771	1,157	1,545	1,934	2,326
15		389	768	1,144	1,526	1,905	2,287
16		366	752	1,140	1,529	1,918	2,313
17		337	732	1,128	1,523	1,905	2,297
18		337	732	1,124	1,513	1,905	2,297
19		431	820	1,215	1,601	1,954	2,381

DECREASING LOAD						
Gage	Load (lb)	Strain ($\mu\epsilon$)				
		120,000	96,000	72,000	48,000	24,000
1		1,970	1,575	1,179	787	399
2		1,928	1,542	1,157	781	399
3		1,947	1,552	1,157	774	389
4		1,931	1,552	1,144	755	366
5		1,814	1,429	1,050	671	298
6		1,889	1,497	1,105	716	327
7		1,798	1,413	1,034	654	279
8		1,869	1,497	1,131	765	405
9		1,983	1,581	1,189	800	408
10		1,918	1,536	1,160	784	408
11		1,950	1,552	1,157	768	379
12		1,970	1,575	1,183	797	408
13		1,921	1,533	1,150	771	389
14		1,923	1,533	1,147	765	379
15		1,899	1,513	1,134	758	382
16		1,912	1,513	1,128	742	353
17		1,928	1,500	1,111	768	324
18		1,892	1,500	1,111	719	324
19		1,980	1,591	1,202	813	421

Strain Gage Data, Panel 1, After Fatigue Test

INCREASING LOAD

Load (lb) Gage	Strain ($\mu\epsilon$)						
	0	24,000	48,000	72,000	96,000	120,000	144,000
1	-36	378	758	1,150	1,539	1,934	2,328
2	-58	356	742	1,128	1,516	1,899	2,284
3	-42	350	735	1,121	1,510	1,902	2,294
4	-19	340	732	1,121	1,510	1,902	2,297
5	-16	272	642	1,017	1,396	1,779	2,158
6	-32	292	677	1,069	1,458	1,850	2,245
7	-26	253	629	1,008	1,303	1,766	2,145
8	-32	389	761	1,140	1,520	1,899	2,284
9	-19	376	765	1,153	1,545	1,941	2,333
10	-6	402	774	1,150	1,529	1,912	2,291
11	-36	343	732	1,124	1,523	1,912	2,310
12	-45	373	765	1,153	1,542	1,934	2,326
13	+266	619	975	1,338	1,714	2,087	2,462
14	-32	343	729	1,118	1,503	1,892	2,284
15	-298	45	399	755	1,118	1,474	1,834
16	-32	324	713	1,098	1,494	1,886	2,281
17	-16	301	703	1,095	1,490	1,886	2,281
18	-45	292	684	1,076	1,468	1,860	2,252
19	-19	402	794	1,183	1,575	1,967	2,524

DECREASING LOAD

Load (lb) Gage	Strain ($\mu\epsilon$)					
	120,000	96,000	72,000	48,000	24,000	0
1	1,940	1,542	1,153	765	376	-29
2	1,900	1,513	1,128	742	356	-55
3	1,910	1,516	1,128	742	356	-36
4	1,910	1,516	1,128	739	350	-19
5	1,780	1,400	1,027	648	275	-16
6	1,860	1,468	1,076	687	301	-29
7	1,770	1,390	1,011	632	259	-26
8	1,900	1,523	1,144	765	389	-26
9	1,940	1,549	1,160	768	382	-13
10	1,910	1,536	1,157	784	408	-0
11	1,920	1,523	1,131	739	353	-32
12	1,940	1,545	1,160	771	382	-36
13	2,080	1,717	1,345	982	625	+259
14	1,900	1,510	1,128	745	356	-29
15	1,480	1,121	761	408	52	-295
16	1,880	1,494	1,108	719	327	-32
17	1,890	1,494	1,102	706	311	-13
18	1,860	1,474	1,085	697	301	-39
19	1,970	1,581	1,189	800	408	-13

RELIABILITY ANALYSIS FATIGUE TEST
 45 DEGREE ROSETTE SINGLE GAGE INSTALLATION
 PANEL N01 STATIC TEST 5-4-1970 THROUGH 5-13-1970

45 DEGREE ROSETTE (SINGLE INSTALLATION)

ROSETTE NUMBER * 20

ET= 10.5 EC= 10.7 POISSONS RATIO = .330

LOAD	LEG STRAINS (100 MICRONS/INCH)		
	LEG *A*	LEG *B*	LEG *C*
OK	0.0	0.0	0.0
24K	3.8	1.5	-.6
48K	7.4	2.8	-1.6
72K	11.0	4.1	-2.6
96K	14.6	5.2	-3.6
120K	18.2	6.6	-4.7
144K	21.9	7.8	-5.8
120K	18.3	6.6	-4.8
96K	14.7	5.3	-3.8
72K	11.1	4.1	-2.7
48K	7.5	2.8	-1.7
24K	3.9	1.5	-.6
OK	0.0	0.0	0.0

LOAD	TRUE STRESSES (KSI)		SHEAR STRESS (KSI) LEG *A* OR *C*
	LEG *A*	LEG *C*	
OK	0.0	0.0	0.0
24K	4.3	.8	-.1
48K	8.1	1.0	-.1
72K	12.0	1.2	-.1
96K	15.8	1.4	-.3
120K	19.7	1.5	-.2
144K	23.5	1.7	-.2
120K	19.7	1.5	-.2
96K	15.9	1.3	-.1
72K	12.0	1.2	-.1
48K	8.2	.9	-.1
24K	4.4	.8	-.1
OK	0.0	0.0	0.0

ROSETTE NUMBER • 20

LOAD	PRINCIPAL STRESSES (KSI)			ANGLE (DEGREES)
	FMAX	FMIN	TMAX	PHI
OK	0.0	0.0	0.0	0.0
24K	4.3	.8	1.7	-46.7
48K	8.1	1.0	3.5	-45.6
72K	12.0	1.2	5.4	-45.6
96K	15.8	1.4	7.2	-46.1
120K	19.7	1.5	9.1	-45.5
144K	23.5	1.7	10.9	-45.5
120K	19.7	1.5	9.1	-45.5
96K	15.9	1.3	7.3	-45.5
72K	12.0	1.1	5.4	-45.6
48K	8.2	.9	3.6	-45.6
24K	4.4	.8	1.8	-46.8
OK	0.0	0.0	0.0	360.0

RELIABILITY ANALYSIS FATIGUE TEST
 45 DEGREE ROSETTE SINGLE GAGE INSTALLATION
 PANEL NO1 STATIC TEST 5-4-1970 THROUGH 5-13-1970

45 DEGREE ROSETTE (SINGLE INSTALLATION)

ROSETTE NUMBER * 21

ET= 10.5 EC= 10.7 POISSONS RATIO = .330

LOAD	LEG STRAINS (100 MICROINCHES/INCH)		
	LEG *A*	LEG *B*	LEG *C*
OK	0.0	0.0	0.0
24K	5.2	1.5	-1.2
48K	9.3	2.8	-2.5
72K	13.5	4.2	-3.7
96K	17.7	5.6	-5.0
120K	21.9	6.9	-6.2
144K	26.0	8.4	-7.5
120K	21.8	6.9	-6.2
96K	17.6	5.5	-5.0
72K	13.4	4.1	-3.7
48K	9.2	2.8	-2.5
24K	5.2	.5	-1.2
OK	0.0	0.0	0.0

LOAD	TRUE STRESSES (KSI)		SHEAR STRESS (KSI) LEG *A* OR *C*
	LEG *A*	LEG *C*	
OK	0.0	0.0	0.0
24K	5.6	.5	-.3
48K	10.0	.6	-.4
72K	14.5	.9	-.5
96K	18.9	1.0	-.6
120K	23.3	1.1	-.7
144K	27.7	1.3	-.7
120K	23.2	1.1	-.7
96K	18.8	1.0	-.7
72K	14.3	.8	-.6
48K	9.9	.7	-.5
24K	5.6	.5	-1.1
OK	0.0	0.0	0.0

ROSETTE NUMBER • 21

LOAD	PRINCIPAL STRESSES (KSI)			ANGLE (DEGREES) PHI
	FMAX	FMIN	TMAX	
OK	0.0	0.0	0.0	0.0
24K	5.6	.5	2.5	-48.7
48K	10.0	.6	4.7	-47.6
72K	14.5	.9	6.8	-47.2
96K	18.9	1.0	9.0	-46.9
120K	23.3	1.1	11.1	-46.8
144K	27.8	1.3	13.2	-46.6
120K	23.2	1.1	11.1	-46.8
96K	18.8	1.0	8.9	-47.1
72K	14.3	.8	6.8	-47.4
48K	10.0	.6	4.7	-48.0
24K	5.8	.3	2.8	-56.9
OK	0.0	0.0	0.0	360.0

RELIABILITY ANALYSIS FATIGUE TEST
45 DEGREE ROSETTE SINGLE GAGE INSTALLATION
PANEL NO1 STATIC TEST 5-4-1970 THROUGH 5-13-1970

45 DEGREE ROSETTE, (SINGLE INSTALLATION)

ROSETTE NUMBER * 22

ET= 10.5 EC= 10.7 POISSONS RATIO = .330

LOAD	LEG STRAINS (100 MICROINCHES/INCH)		
	LEG *A*	LEG *B*	LEG *C*
OK	0.0	0.0	0.0
24K	3.5	1.3	-.6
48K	7.3	2.7	-1.7
72K	11.1	4.1	-2.9
96K	14.9	5.4	-4.1
120K	18.7	6.8	-5.3
144K	22.8	8.1	-6.5
120K	18.7	6.8	-5.3
96K	14.9	5.4	-4.1
72K	11.1	4.1	-2.9
48K	9.2	2.7	-1.7
24K	3.6	1.4	-.5
OK	0.0	0.0	0.0

LOAD	TRUE STRESSES (KSI)		SHEAR STRESS (KSI) LEG *A* OR *C*
	LEG *A*	LEG *C*	
OK	0.0	0.0	0.0
24K	3.9	.7	-.1
48K	7.9	.8	-.1
72K	11.9	.9	-.0
96K	15.9	1.0	.0
120K	20.0	1.0	.0
144K	24.4	1.3	-.1
120K	20.0	1.0	.0
96K	16.0	1.0	-.0
72K	12.0	.9	-.0
48K	10.2	1.6	-.8
24K	4.0	.7	-.1
OK	0.0	0.0	0.0

ROSETTE NUMBER # 22

LOAD	PRINCIPAL STRESSES (KSI)			ANGLE (DEGREES)
	FMAX	FMIN	TMAX	PHI
OK	0.0	0.0	0.0	0.0
24K	3.9	.7	1.6	-46.8
48K	7.9	.8	3.6	-45.5
72K	11.9	.9	5.5	-45.1
96K	15.9	1.0	7.5	-45.0
120K	20.0	1.0	9.5	-44.9
144K	24.4	1.3	11.6	-45.1
120K	20.0	1.0	9.5	-44.9
96K	16.0	1.0	7.5	-45.0
72K	12.0	.9	5.5	-45.2
48K	10.3	1.5	4.4	-50.4
24K	4.0	.7	1.6	-46.8
OK	0.0	0.0	0.0	360.0

RELIABILITY ANALYSIS FATIGUE TEST
45 DEGREE ROSETTE SINGLE GAGE INSTALLATION
PANEL NO1 STATIC TEST 5-4-1970 THROUGH 5-13-1970

45 DEGREE ROSETTE (SINGLE INSTALLATION)

ROSETTE NUMBER * 23

ET= 10.5 EC= 10.7 POISSONS RATIO = .330

LOAD	LEG STRAINS (100 MICROINCHES/INCH)		
	LEG *A*	LEG *B*	LEG *C*
OK	0.0	0.0	0.0
24K	3.7	1.3	-1.1
48K	7.6	2.6	-2.3
72K	11.5	4.0	-3.5
96K	15.4	5.3	-4.8
120K	19.3	6.6	-6.0
144K	23.2	7.9	-7.2
120K	19.3	6.6	-6.0
96K	15.4	5.3	-4.7
72K	11.5	4.0	-3.5
48K	7.6	2.7	-2.3
24K	3.7	1.4	-1.1
OK	0.0	0.0	0.0

LOAD	TRUE STRESSES (KSI)		SHEAR STRESS (KSI) LEG *A* OR *C*
	LEG *A*	LEG *C*	
OK	0.0	0.0	0.0
24K	3.9	.1	.0
48K	8.0	.2	.0
72K	12.1	.3	.0
96K	16.3	.4	-.0
120K	20.4	.4	-.1
144K	24.6	.5	-.1
120K	20.4	.4	-.0
96K	16.3	.4	-.0
72K	12.2	.3	.0
48K	8.0	.2	.0
24K	4.0	.2	.1
OK	0.0	0.0	0.0

ROSETTE NUMBER * 23

LOAD	PRINCIPAL STRESSES (KSI)			ANGLE (DEGREES)
	FMAX	FMIN	TMAX	PHI
OK	0.0	0.0	0.0	0.0
24K	3.9	.1	1.9	-44.6
48K	8.0	.2	3.9	-44.9
72K	12.1	.3	5.9	-44.9
96K	16.3	.4	8.0	-45.1
120K	20.4	.4	10.0	-45.1
144K	24.6	.5	12.0	-45.2
120K	20.4	.4	10.0	-45.0
96K	16.3	.4	7.9	-45.0
72K	12.2	.3	5.9	-44.9
48K	8.0	.2	3.9	-44.9
24K	4.0	.2	1.9	-44.2
OK	0.0	0.0	0.0	360.0

RELIABILITY ANALYSIS FATIGUE TEST
 45 DEGREE ROSETTE SINGLE GAGE INSTALLATION
 PANEL NO1 STATIC TEST 5-4-1970 THROUGH 5-13-1970

45 DEGREE ROSETTE (SINGLE INSTALLATION)

ROSETTE NUMBER * 24

ET= 10.5 EC= 10.7 POISSONS RATIO = .330

LOAD	LEG STRAINS (100 MICROINCHES/INCH)		
	LEG *A*	LEG *B*	LEG *C*
OK	0.0	0.0	0.0
24K	3.6	1.3	-1.0
48K	7.1	2.5	-1.7
72K	10.7	3.8	-2.8
96K	14.3	5.1	-3.8
120K	18.0	6.3	-4.9
144K	21.7	7.6	-5.9
120K	18.0	6.3	-4.9
96K	14.4	5.0	-3.9
72K	10.8	3.8	-2.9
48K	7.2	2.5	-1.9
24K	3.6	1.3	-0.8
OK	0.0	0.0	0.0

LOAD	TRUE STRESSES (KSI)		SHEAR STRESS (KSI)
	LEG *A*	LEG *C*	LEG *A* OR *C*
OK	0.0	0.0	0.0
24K	3.8	.2	.0
48K	7.7	.8	-.1
72K	11.6	.9	-.1
96K	15.4	1.0	-.1
120K	19.3	1.2	-.2
144K	23.2	1.5	-.2
120K	19.3	1.2	-.2
96K	15.4	1.0	-.2
72K	11.6	.8	-.1
48K	7.8	.6	-.1
24K	3.9	.5	-.1
OK	0.0	0.0	0.0

ROSETTE NUMBER * 24

LOAD	PRINCIPAL STRESSES (KSI)			ANGLE (DEGREES) PHI
	FMAX	FMIN	TMAX	
OK	0.0	0.0	0.0	0.0
24K	3.8	.2	1.8	-44.4
48K	7.7	.7	3.5	-46.0
72K	11.6	.9	5.3	-45.7
96K	15.4	1.0	7.2	-45.5
120K	19.3	1.2	9.0	-45.5
144K	23.2	1.5	10.9	-45.6
120K	19.3	1.2	9.1	-45.6
96K	15.4	1.0	7.2	-45.7
72K	11.6	.8	5.4	-45.7
48K	7.8	.6	3.6	-45.9
24K	4.0	.5	1.7	-46.7
OK	0.0	0.0	0.0	360.0

RELIABILITY ANALYSIS FATIGUE TEST
45 DEGREE ROSETTE SINGLE GAGE INSTALLATION
PANEL NO1 STATIC TEST 5-4-1970 THROUGH 5-13-1970

45 DEGREE ROSETTE (SINGLE INSTALLATION)

ROSETTE NUMBER * 25

ET= 10.5 EC= 10.7 POISSONS RATIO = .330

LOAD	LEG STRAINS (100 MICROINCHES/INCH)		
	LEG *A*	LEG *B*	LEG *C*
OK	0.0	0.0	0.0
24K	4.9	1.3	-1.5
48K	9.1	2.6	-2.8
72K	13.2	4.0	-4.0
96K	17.3	5.3	-5.2
120K	21.6	6.7	-6.5
144K	25.8	8.1	-7.7
120K	21.5	6.6	-6.5
96K	17.2	5.2	-5.2
72K	13.1	3.8	-4.0
48K	9.0	2.4	-2.8
24K	4.8	1.2	-1.5
OK	0.0	0.0	0.0

LOAD	TRUE STRESSES (KSI)		SHEAR STRESS (KSI) LEG *A* OR *C*
	LEG *A*	LEG *C*	
OK	0.0	0.0	0.0
24K	5.2	.2	-.3
48K	9.6	.3	-.5
72K	14.0	.4	-.5
96K	18.4	.6	-.6
120K	22.9	.7	-.7
144K	27.4	1.0	-.7
120K	22.8	.7	-.7
96K	18.2	.5	-.7
72K	13.9	.3	-.6
48K	9.5	.2	-.5
24K	5.1	.1	-.4
OK	0.0	0.0	0.0

ROSETTE NUMBER * 25

LOAD	PRINCIPAL STRESSES (KSI)			ANGLE (DEGREES)
	FMAX	FMIN	TMAX	PHI
OK	0.0	0.0	0.0	0.0
24K	5.2	.1	2.5	-48.6
48K	9.6	.3	4.7	-47.7
72K	14.0	.4	6.8	-47.1
96K	18.4	.6	8.9	-46.9
120K	22.9	.7	11.1	-46.7
144K	27.4	1.0	13.2	-46.6
120K	22.8	.7	11.0	-46.8
96K	18.3	.5	8.9	-47.1
72K	13.9	.3	6.8	-47.4
48K	9.5	.2	4.7	-48.2
24K	5.1	.1	2.5	-49.2
OK	0.0	0.0	0.0	360.0

RELIABILITY ANALYSIS FATIGUE TEST
 45 DEGREE ROSETTE SINGLE GAGE INSTALLATION
 PANEL NO1 STATIC TEST 5-4-1970 THROUGH 5-13-1970

45 DEGREE ROSETTE (SINGLE INSTALLATION)

ROSETTE NUMBER * 26

ET= 10.5 EC= 10.7 POISSONS RATIO = .330

LOAD	LEG STRAINS (100 MICROINCHES/INCH)		
	LEG *A*	LEG *B*	LEG *C*
OK	0.0	0.0	0.0
24K	3.3	1.2	-1.1
48K	7.0	2.4	-2.0
72K	10.8	3.8	-3.1
96K	14.6	5.2	-5.0
120K	18.5	6.5	-5.5
144K	22.4	7.9	-6.6
120K	18.5	6.5	-5.5
96K	14.6	5.1	-4.3
72K	10.8	3.8	-3.1
48K	7.1	2.4	-2.0
24K	3.3	1.1	-1.1
OK	0.0	0.0	0.0

LOAD	TRUE STRESSES (KSI)		SHEAR STRESS (KSI) LEG *A* OR *C*
	LEG *A*	LEG *C*	
OK	0.0	0.0	0.0
24K	3.5	.0	.0
48K	7.5	.4	-.1
72K	11.6	.6	-.1
96K	15.3	-.2	.3
120K	19.7	.7	.0
144K	23.8	.9	.0
120K	19.6	.7	.0
96K	15.5	.6	-.0
72K	11.6	.5	-.1
48K	7.6	.4	-.1
24K	3.5	-.0	.0
OK	0.0	0.0	0.0

ROSETTE NUMBER * 26

LOAD	PRINCIPAL STRESSES (KSI)			ANGLE (DEGREES)
	FMAX	FMIN	TMAX	PHI
OK	0.0	0.0	0.0	0.0
24K	3.5	.0	1.7	-44.6
48K	7.5	.4	3.6	-45.7
72K	11.6	.6	5.5	-45.3
96K	15.3	-.2	7.7	-44.1
120K	19.7	.7	9.5	-45.0
144K	23.8	.9	11.4	-44.9
120K	19.6	.7	9.4	-44.9
96K	15.5	.6	7.5	-45.0
72K	11.6	.5	5.5	-45.3
48K	7.6	.4	3.6	-46.0
24K	3.5	-.0	1.7	-44.8
OK	0.0	0.0	0.0	360.0

RELIABILITY ANALYSIS FATIGUE TEST
 45 DEGREE ROSETTE SINGLE GAGE INSTALLATION
 PANEL N01 STATIC TEST 5-4-1970 THROUGH 5-13-1970

45 DEGREE ROSETTE (SINGLE INSTALLATION)

ROSETTE NUMBER * 27

ET= 10.5 EC= 10.7 POISSONS RATIO = .330

LOAD	LEG STRAINS (100 MICROINCHES/INCH)		
	LEG *A*	LEG *B*	LEG *C*
OK	0.0	0.0	0.0
24K	3.4	1.1	-1.3
48K	7.2	2.4	-2.6
72K	11.1	3.7	-3.8
96K	15.0	5.0	-5.0
120K	19.0	6.3	-6.2
144K	22.9	7.7	-7.4
120K	18.9	6.3	-6.2
96K	15.0	5.0	-5.0
72K	11.1	3.7	-3.7
48K	7.3	2.4	-2.5
24K	3.4	1.1	-1.3
OK	0.0	0.0	0.0

LOAD	TRUE STRESSES (KSI)		SHEAR STRESS (KSI) LEG *A* OR *C*
	LEG *A*	LEG *C*	
OK	0.0	0.0	0.0
24K	3.5	-.2	.1
48K	7.5	-.2	.0
72K	11.6	-.1	.0
96K	15.8	-.0	-.0
120K	20.0	.0	-.0
144K	24.2	.2	-.1
120K	19.9	.1	-.1
96K	15.7	-.0	-.0
72K	11.7	-.1	.0
48K	7.6	-.2	.0
24K	3.5	-.2	.1
OK	0.0	0.0	0.0

ROSETTE NUMBER * 27

LOAD	PRINCIPAL STRESSES (KSI)			ANGLE (DEGREES)
	FMAX	FMIN	TMAX	PHI
OK	0.0	0.0	0.0	0.0
24K	3.5	-.2	1.9	-44.0
48K	7.5	-.2	3.9	-44.8
72K	11.6	-.1	5.9	-44.8
96K	15.8	-.0	7.9	-45.1
120K	20.0	.0	10.0	-45.1
144K	24.2	.2	12.0	-45.2
120K	19.9	.1	9.9	-45.1
96K	15.7	-.0	7.9	-45.0
72K	11.7	-.1	5.9	-44.9
48K	7.6	-.2	3.9	-45.0
24K	3.5	-.2	1.9	-44.2
OK	0.0	0.0	0.0	360.0

RELIABILITY ANALYSIS FATIGUE TEST
 45 DEGREE ROSETTE SINGLE GAGE INSTALLATION
 PANEL NO1 STATIC TEST 5-4-1970 THROUGH 5-13-1970

45 DEGREE ROSETTE (SINGLE INSTALLATION)

ROSETTE NUMBER * 28

ET= 10.5 EC= 10.7 POISSONS RATIO = .330

LOAD	LEG STRAINS (100 MICROINCHES/INCH)		
	LEG *A*	LEG *B*	LEG *C*
OK	0.0	0.0	0.0
24K	3.6	1.3	-1.7
48K	7.1	2.6	-3.8
72K	10.7	3.8	-5.9
96K	14.4	5.1	-7.9
120K	18.0	6.3	-9.9
144K	21.7	7.6	-11.9
120K	18.1	6.4	-9.9
96K	14.5	5.2	-7.9
72K	10.9	3.9	-5.9
48K	7.2	2.6	-3.8
24K	3.6	1.3	-1.7
OK	0.0	0.0	0.0

LOAD	TRUE STRESSES (KSI)		SHEAR STRESS (KSI) LEG *A* OR *C*
	LEG *A*	LEG *C*	
OK	0.0	0.0	0.0
24K	3.9	.5	-1.1
48K	7.7	.7	-1.1
72K	11.6	.9	-1.1
96K	15.5	1.1	-1.2
120K	19.3	1.3	-1.2
144K	23.2	1.5	-1.2
120K	19.5	1.4	-1.2
96K	15.6	1.1	-1.2
72K	11.8	1.0	-1.2
48K	7.8	.7	-1.1
24K	4.0	.5	-1.1
OK	0.0	0.0	0.0

ROSETTE NUMBER * 28

LOAD	PRINCIPAL STRESSES (KSI)			ANGLE (DEGREES)
	FMAX	FMIN	TMAX	PHI
OK	0.0	0.0	0.0	0.0
24K	3.9	.5	1.7	-46.5
48K	7.7	.7	3.5	-45.9
72K	11.6	.9	5.3	-45.7
96K	15.5	1.1	7.2	-45.7
120K	19.3	1.3	9.0	-45.6
144K	23.2	1.5	10.9	-45.6
120K	19.5	1.4	9.1	-45.6
96K	15.6	1.1	7.2	-45.6
72K	11.8	1.0	5.4	-45.8
48K	7.8	.7	3.6	-46.1
24K	4.0	.5	1.7	-46.9
OK	0.0	0.0	0.0	360.0

RELIABILITY ANALYSIS FATIGUE TEST
 45 DEGREE ROSETTE SINGLE GAGE INSTALLATION
 PANEL NO1 STATIC TEST 5-4-1970 THROUGH 5-13-1970

45 DEGREE ROSETTE (SINGLE INSTALLATION)

ROSETTE NUMBER * 29

ET= 10.5 EC= 10.7 POISSONS RATIO = .330

LOAD	LEG STRAINS (100 MICROINCHES/INCH)		
	LEG *A*	LEG *B*	LEG *C*
OK	0.0	0.0	0.0
24K	4.9	1.3	-1.5
48K	9.1	2.6	-2.7
72K	13.2	4.0	-4.0
96K	17.4	5.3	-5.2
120K	21.6	6.8	-6.4
144K	25.8	8.2	-7.6
120K	21.6	6.7	-6.3
96K	17.3	5.3	-5.1
72K	13.1	3.9	-3.9
48K	9.0	2.5	-2.7
24K	4.8	1.2	-1.5
OK	0.0	0.0	0.0

LOAD	TRUE STRESSES (KSI)		SHEAR STRESS (KSI) LEG *A* OR *C*
	LEG *A*	LEG *C*	
OK	0.0	0.0	0.0
24K	5.2	.2	-.4
48K	9.7	.3	-.5
72K	14.1	.4	-.5
96K	18.5	.7	-.7
120K	23.0	.8	-.7
144K	27.5	1.1	-.7
120K	23.0	.9	-.7
96K	18.5	.7	-.7
72K	13.9	.5	-.6
48K	9.5	.3	-.5
24K	5.1	.1	-.4
OK	0.0	0.0	0.0

ROSETTE NUMBER • 29

LOAD	PRINCIPAL STRESSES (KSI)			ANGLE (DEGREES)
	FMAX	FMIN	TMAX	PHI
OK	0.0	0.0	0.0	0.0
24K	5.3	.2	2.6	-49.0
48K	9.7	.3	4.7	-47.9
72K	14.1	.4	6.8	-47.2
96K	18.6	.6	9.0	-47.1
120K	23.0	.8	11.1	-46.7
144K	27.5	1.0	13.2	-46.6
120K	23.0	.9	11.0	-46.8
96K	18.5	.7	8.9	-47.2
72K	14.0	.5	6.7	-47.5
48K	9.5	.3	4.6	-48.3
24K	5.1	.1	2.5	-49.4
OK	0.0	0.0	0.0	360.0

RELIABILITY ANALYSIS FATIGUE TEST
 45 DEGREE ROSETTE SINGLE GAGE INSTALLATION
 PANEL NO1 STATIC TEST 5-4-1970 THROUGH 5-13-1970

45 DEGREE ROSETTE (SINGLE INSTALLATION)

ROSETTE NUMBER * 30

ET= 10.5 EC= 10.7 POISSONS RATIO = .330

LOAD	LEG STRAINS (100 MICROINCHES/INCH)		
	LEG *A*	LEG *B*	LEG *C*
OK	0.0	0.0	0.0
24K	3.3	1.1	-.7
48K	7.1	2.5	-1.9
72K	10.8	3.8	-3.1
96K	14.7	5.2	-4.2
120K	18.5	6.6	-5.4
144K	22.4	8.0	-6.5
120K	18.6	6.7	-5.3
96K	14.8	5.2	-4.2
72K	10.9	3.8	-3.1
48K	7.1	2.5	-1.9
24K	3.4	1.1	-.7
OK	0.0	0.0	0.0

LOAD	TRUE STRESSES (KSI)		SHEAR STRESS (KSI) LEG *A* OR *C*
	LEG *A*	LEG *C*	
OK	0.0	0.0	0.0
24K	3.6	.4	-.1
48K	7.6	.5	-.1
72K	11.6	.6	-.0
96K	15.6	.7	-.0
120K	19.7	.8	0.0
144K	23.8	1.0	.1
120K	19.8	.9	.0
96K	15.8	.8	-.1
72K	11.7	.6	-.1
48K	7.7	.6	-.1
24K	3.7	.4	-.2
OK	0.0	0.0	0.0

ROSETTE NUMBER * 30

LOAD	PRINCIPAL STRESSES (KSI)			ANGLE (DEGREES)
	FMAX	FMIN	TMAX	PHI
OK	0.0	0.0	0.0	0.0
24K	3.6	.4	1.6	-47.3
48K	7.6	.5	3.6	-45.7
72K	11.6	.6	5.5	-45.2
96K	15.6	.7	7.5	-45.1
120K	19.7	.8	9.4	-45.0
144K	23.8	1.0	11.4	-44.8
120K	19.8	.9	9.4	-44.9
96K	15.8	.8	7.5	-45.4
72K	11.7	.6	5.5	-45.3
48K	7.7	.5	3.6	-45.8
24K	3.7	.4	1.6	-47.7
OK	0.0	0.0	0.0	360.0

RELIABILITY ANALYSIS FATIGUE TEST
 45 DEGREE ROSETTE SINGLE GAGE INSTALLATION
 PANEL NO1 STATIC TEST 5-4-1970 THROUGH 5-13-1970

45 DEGREE ROSETTE (SINGLE INSTALLATION)

ROSETTE NUMBER * 31

ET= 10.5 EC= 10.7 POISSONS RATIO = .330

LOAD	LEG STRAINS (100 MICROINCHES/INCH)		
	LEG *A*	LEG *B*	LEG *C*
OK	0.0	0.0	0.0
24K	3.4	1.2	-1.3
48K	7.3	2.4	-2.5
72K	11.2	3.8	-3.7
96K	15.1	5.1	-4.9
120K	19.0	6.4	-6.1
144K	23.1	7.8	-7.3
120K	19.1	6.5	-6.0
96K	15.1	5.1	-4.8
72K	11.2	3.8	-3.6
48K	7.3	2.4	-2.5
24K	3.4	1.1	-1.2
OK	0.0	0.0	0.0

LOAD	TRUE STRESSES (KSI)		SHEAR STRESS (KSI) LEG *A* OR *C*
	LEG *A*	LEG *C*	
OK	0.0	0.0	0.0
24K	3.5	-.2	.1
48K	7.6	-.1	.0
72K	11.8	-.0	.0
96K	15.9	.1	-.0
120K	20.1	.2	-.1
144K	24.4	.4	-.1
120K	20.2	.3	-.1
96K	16.0	.2	-.1
72K	11.8	.1	.0
48K	7.6	-.1	-.0
24K	3.5	-.1	.0
OK	0.0	0.0	0.0

ROSETTE NUMBER * 31

LOAD	PRINCIPAL STRESSES (KSI)			ANGLE (DEGREES)
	FMAX	FMIN	TMAX	PHI
OK	0.0	0.0	0.0	0.0
24K	3.5	-.2	1.9	-43.8
48K	7.6	-.1	3.9	-44.8
72K	11.8	-.0	5.9	-44.9
96K	15.9	.1	7.9	-45.1
120K	20.1	.2	9.9	-45.1
144K	24.4	.4	12.0	-45.2
120K	20.2	.3	9.9	-45.2
96K	16.0	.2	7.9	-45.2
72K	11.8	.1	5.9	-45.0
48K	7.6	-.1	3.9	-45.1
24K	3.5	-.1	1.8	-44.6
OK	0.0	0.0	0.0	360.0

RELIABILITY ANALYSIS FATIGUE TEST
 45 DEGREE ROSETTE SINGLE GAGE INSTALLATION
 PANEL NO1 STATIC TEST 5-4-1970 THROUGH 5-13-1970

45 DEGREE ROSETTE (SINGLE INSTALLATION)

ROSETTE NUMBER * 32

ET= 10.5 EC= 10.7 POISSONS RATIO = .330

LOAD	LEG STRAINS (100 MICROINCHES/INCH)		
	LEG *A*	LEG *B*	LEG *C*
OK	0.0	0.0	0.0
24K	3.5	1.3	-.6
48K	6.9	2.5	-1.6
72K	10.5	3.7	-2.7
96K	14.1	5.0	-3.6
120K	17.7	6.3	-4.7
144K	21.3	7.6	-5.7
120K	17.8	6.3	-4.7
96K	14.2	5.1	-3.7
72K	10.7	3.8	-2.7
48K	7.1	2.5	-1.7
24K	3.6	1.3	-.7
OK	0.0	0.0	0.0

LOAD	TRUE STRESSES (KSI)		SHEAR STRESS (KSI) LEG *A* OR *C*
	LEG *A*	LEG *C*	
OK	0.0	0.0	0.0
24K	3.9	.6	-.1
48K	7.5	.8	-.1
72K	11.3	1.0	-.1
96K	15.2	1.2	-.2
120K	19.1	1.4	-.2
144K	22.9	1.6	-.2
120K	19.2	1.4	-.2
96K	15.3	1.2	-.1
72K	11.5	.9	-.1
48K	7.7	.8	-.1
24K	3.9	.6	-.1
OK	0.0	0.0	0.0

ROSETTE NUMBER * 32

LOAD	PRINCIPAL STRESSES (KSI)			ANGLE (DEGREES)
	FMAX	FMIN	TMAX	PHI
OK	0.0	0.0	0.0	0.0
24K	3.9	.6	1.6	-47.0
48K	7.6	.8	3.4	-46.1
72K	11.3	.9	5.2	-45.8
96K	15.2	1.2	7.0	-45.8
120K	19.1	1.3	8.9	-45.6
144K	22.9	1.5	10.7	-45.5
120K	19.2	1.4	8.9	-45.7
96K	15.3	1.2	7.1	-45.6
72K	11.5	.9	5.3	-45.7
48K	7.7	.8	3.5	-46.2
24K	3.9	.6	1.7	-46.3
OK	0.0	0.0	0.0	360.0

RELIABILITY ANALYSIS FATIGUE TEST
45 DEGREE ROSETTE SINGLE GAGE INSTALLATION
PANEL NO1 STATIC TEST 5-4-1970 THROUGH 5-13-1970

45 DEGREE ROSETTE (SINGLE INSTALLATION)

ROSETTE NUMBER * 33

ET= 10.5 EC= 10.7 POISSONS RATIO = .330

LOAD	LEG STRAINS (100 MICROINCHES/INCH)		
	LEG *A*	LEG *B*	LEG *C*
OK	0.0	0.0	0.0
24K	5.0	1.3	-1.4
48K	9.1	2.6	-2.6
72K	13.2	3.9	-3.9
96K	17.3	5.3	-5.2
120K	21.5	6.8	-6.4
144K	25.7	8.1	-7.6
120K	21.4	6.7	-6.3
96K	17.3	5.3	-5.1
72K	13.2	3.9	-3.8
48K	9.1	2.6	-2.6
24K	5.0	1.3	-1.3
OK	.1	.1	.0

LOAD	TRUE STRESSES (KSI)		SHEAR STRESS (KSI) LEG *A* OR *C*
	LEG *A*	LEG *C*	
OK	0.0	0.0	0.0
24K	5.4	.3	-.4
48K	9.7	.4	-.5
72K	14.0	.5	-.6
96K	18.4	.7	-.6
120K	22.8	.8	-.6
144K	27.3	1.0	-.7
120K	22.8	.9	-.7
96K	18.4	.8	-.7
72K	14.0	.6	-.6
48K	9.7	.5	-.5
24K	5.4	.4	-.4
OK	.1	.1	.0

ROSETTE NUMBER * 33

LOAD	PRINCIPAL STRESSES (KSI)			ANGLE (DEGREES)
	FMAX	FMIN	TMAX	PHI
OK	0.0	0.0	0.0	0.0
24K	5.4	.3	2.6	-49.3
48K	9.7	.4	4.6	-47.9
72K	14.0	.5	6.8	-47.3
96K	18.5	.7	8.9	-46.9
120K	22.8	.8	11.0	-46.6
144K	27.3	1.0	13.2	-46.5
120K	22.8	.8	11.0	-46.8
96K	18.5	.8	8.9	-47.1
72K	14.0	.6	6.7	-47.4
48K	9.7	.5	4.6	-48.2
24K	5.4	.3	2.5	-49.3
OK	.1	.1	.0	-45.0

RELIABILITY ANALYSIS FATIGUE TEST
45 DEGREE ROSETTE SINGLE GAGE INSTALLATION
PANEL NO1 STATIC TEST 5-4-1970 THROUGH 5-13-1970

45 DEGREE ROSETTE (SINGLE INSTALLATION)

ROSETTE NUMBER * 34

ET= 10.5 EC= 10.7 POISSONS RATIO = .330

LOAD	LEG STRAINS (100 MICROINCHES/INCH)		
	LEG *A*	LEG *B*	LEG *C*
OK	0.0	0.0	0.0
24K	3.7	1.2	-.8
48K	7.5	2.5	-1.9
72K	11.2	3.9	-3.0
96K	15.0	5.3	-4.2
120K	18.8	6.6	-5.4
144K	22.7	8.0	-6.6
120K	18.9	6.6	-5.3
96K	15.1	5.3	-4.2
72K	11.3	3.9	-3.1
48K	7.5	2.6	-1.9
24K	3.8	1.2	-.7
OK	0.0	.0	0.0

LOAD	TRUE STRESSES (KSI)		SHEAR STRESS (KSI) LEG *A* OR *C*
	LEG *A*	LEG *C*	
OK	0.0	0.0	0.0
24K	4.1	.6	-.2
48K	8.0	.6	-.2
72K	12.1	.8	-.2
96K	16.0	.9	-.1
120K	20.1	1.0	-.1
144K	24.2	1.1	-.1
120K	20.2	1.0	-.1
96K	16.1	.9	-.1
72K	12.1	.8	-.1
48K	8.1	.7	-.2
24K	4.2	.6	-.2
OK	0.0	0.0	.0

ROSETTE NUMBER * 34

LOAD	PRINCIPAL STRESSES (KSI)			ANGLE (DEGREES)
	FMAX	FMIN	TMAX	PHI
OK	0.0	0.0	0.0	0.0
24K	4.1	.5	1.8	-48.8
48K	8.0	.6	3.7	-46.5
72K	12.1	.8	5.6	-45.9
96K	16.0	.9	7.6	-45.3
120K	20.1	1.0	9.5	-45.2
144K	24.2	1.1	11.6	-45.2
120K	20.2	1.0	9.6	-45.3
96K	16.1	.9	7.6	-45.4
72K	12.1	.8	5.7	-45.6
48K	8.1	.7	3.7	-46.5
24K	4.2	.6	1.8	-48.7
OK	.0	-0.0	.0	0.0

RELIABILITY ANALYSIS FATIGUE TEST
 45 DEGREE ROSETTE SINGLE GAGE INSTALLATION
 PANEL N01 STATIC TEST 5-4-1970 THROUGH 5-13-1970

45 DEGREE ROSETTE (SINGLE INSTALLATION)

ROSETTE NUMBER * 35

ET= 10.5 EC= 10.7 POISSONS RATIO = .330

LOAD	LEG STRAINS (100 MICROINCHES/INCH)		
	LEG *A*	LEG *B*	LEG *C*
OK	0.0	0.0	0.0
24K	3.6	1.1	-1.2
48K	7.4	2.4	-2.4
72K	11.3	3.7	-3.5
96K	15.2	5.0	-4.7
120K	19.1	6.4	-5.9
144K	23.1	7.7	-7.0
120K	19.2	6.4	-5.8
96K	15.3	5.1	-4.6
72K	11.4	3.8	-3.5
48K	7.6	2.5	-2.3
24K	3.7	1.2	-1.2
OK	.0	.0	.0

LOAD	TRUE STRESSES (KSI)		SHEAR STRESS (KSI) LEG *A* OR *C*
	LEG *A*	LEG *C*	
OK	0.0	0.0	0.0
24K	3.8	-.0	-.1
48K	7.8	.1	-.1
72K	11.9	.2	-.2
96K	16.1	.4	-.2
120K	20.3	.5	-.2
144K	24.5	.7	-.2
120K	20.3	.6	-.2
96K	16.3	.5	-.2
72K	12.1	.4	-.2
48K	8.0	.2	-.1
24K	3.9	.1	-.1
OK	.1	.1	.0

ROSETTE NUMBER * 35

LOAD	PRINCIPAL STRESSES (KSI)			ANGLE (DEGREES)
	FMAX	FMIN	TMAX	PHI
OK	0.0	0.0	0.0	0.0
24K	3.8	-.0	1.9	-46.7
48K	7.8	.1	3.9	-45.9
72K	11.9	.2	5.9	-45.8
96K	16.1	.4	7.9	-45.7
120K	20.3	.5	9.9	-45.6
144K	24.5	.7	11.9	-45.5
120K	20.3	.6	9.9	-45.7
96K	16.3	.5	7.9	-45.7
72K	12.1	.4	5.9	-45.7
48K	8.0	.2	3.9	-45.9
24K	3.9	.1	1.9	-46.5
OK	.1	.1	.0	-22.5

Strain Gage Locations on Panel 2

Gage	Location				Type	
	x (in.)	y (in.)	Drill entry side	Drill exit side	Uniaxial	Rosette
1	-21	35	●		●	
2	0	35	●		●	
3	+21	35	●		●	
4	-21	35		●	●	
5	0	35		●	●	
6	+21	35		●	●	
7	0	72	●		●	
8	0	72		●	●	
9	-21	109	●		●	
10	0	109	●		●	
11	+21	109	●		●	
18	+20.8	72	●		●	

Strain Gage Data, Panel 2, First Cycle Before Fatigue Test

INCREASING LOAD

		Strain ($\mu\epsilon$)						
Load (lb) Gage	0	24,000	48,000	72,000	96,000	120,000	144,000	
1	26	456	844	1,239	1,630	2,025	2,420	
2	23	469	854	1,236	1,618	2,002	2,387	
3	49	466	861	1,255	1,653	2,051	2,451	
4	19	404	802	1,197	1,592	1,990	2,387	
5	10	298	676	1,055	1,436	1,821	2,203	
6	19	398	789	1,187	1,585	1,990	2,391	
7	0	346	728	1,110	1,495	1,883	2,271	
8	29	446	828	1,213	1,595	1,983	2,371	
9	55	466	854	1,245	1,630	2,025	2,420	
10	0	427	802	1,181	1,556	1,941	2,323	
11	49	450	834	1,223	1,614	2,009	2,400	
18	3	362	754	1,148	1,546	1,947	2,342	

DECREASING LOAD

		Strain ($\mu\epsilon$)				
Load (lb) Gage	120,000	96,000	72,000	48,000	24,000	0
1	2,022	1,630	1,236	848	459	32
2	2,002	1,621	1,239	857	476	29
3	2,054	1,656	1,262	867	476	58
4	1,990	1,592	1,200	806	414	26
5	1,818	1,436	1,058	679	304	16
6	1,990	1,588	1,194	799	404	29
7	1,880	1,498	1,113	731	349	6
8	1,983	1,595	1,213	831	450	36
9	2,025	1,630	1,239	854	466	58
10	1,941	1,563	1,187	809	430	29
11	2,012	1,618	1,229	844	456	55
18	1,947	1,546	1,155	760	366	13

Strain Gage Data, Panel 2, Second Cycle Before Fatigue Test

INCREASING LOAD

Load (lb) Gage	Strain ($\mu\epsilon$)						
	0	24,000	48,000	72,000	96,000	120,000	144,000
1	32	460	847	1,240	1,634	2,028	2,426
2	29	476	857	1,240	1,621	2,006	2,394
3	58	476	876	1,250	1,656	2,057	2,459
4	26	418	810	1,200	1,598	1,996	2,394
5	16	304	680	1,060	1,436	1,821	2,206
6	29	405	756	1,190	1,592	1,996	2,397
7	6	350	730	1,110	1,498	1,886	2,271
8	36	450	831	1,210	1,598	1,990	2,374
9	58	470	857	1,250	1,627	2,028	2,423
10	29	430	805	1,180	1,563	1,944	2,326
11	55	456	838	1,230	1,521	2,012	2,407
18	13	379	756	1,150	1,553	1,951	2,349

DECREASING LOAD

Load (lb) Gage	Strain ($\mu\epsilon$)					
	120,000	96,000	72,000	48,000	24,000	0
1	2,025	1,634	1,239	851	463	36
2	2,006	1,624	1,242	864	479	32
3	2,057	1,663	1,265	873	479	61
4	1,993	1,598	1,203	812	417	29
5	1,821	1,443	1,061	682	307	16
6	1,996	1,595	1,200	802	404	29
7	1,886	1,501	1,116	734	353	3
8	1,986	1,601	1,216	835	453	42
9	2,025	1,634	1,245	854	469	65
10	1,944	1,566	1,190	812	433	0
11	2,012	1,624	1,236	848	459	61
18	1,967	1,556	1,161	763	369	3

Strain Gage Data, Panel 2, After Fatigue Test

INCREASING LOAD

Load (lb) Gage	Strain ($\mu\epsilon$)						
	0	24,000	48,000	72,000	96,000	120,000	144,000
1	0	434	825	1,220	1,610	2,010	2,400
2	10	456	846	1,230	1,610	2,000	2,380
3	10	437	831	1,230	1,620	2,030	2,420
4	0	388	783	1,180	1,570	1,970	2,370
5	0	288	670	1,060	1,420	1,810	2,180
6	0	366	764	1,160	1,580	1,980	2,360
7	0	343	728	1,110	1,490	1,890	2,280
8	16	440	828	1,210	1,600	1,990	2,380
9	19	440	831	1,220	1,610	2,010	2,400
10	0	415	798	1,170	1,550	1,930	2,310
11	16	424	809	1,200	1,580	1,980	2,370
18	---	---	---	---	---	---	---

DECREASING LOAD

Load (lb) Gage	Strain ($\mu\epsilon$)					
	120,000	96,000	72,000	48,000	24,000	0
1	2,008	1,608	1,216	622	434	0
2	1,990	1,575	1,226	841	459	13
3	2,022	1,621	1,226	828	437	16
4	1,967	1,566	1,174	780	385	0
5	1,808	1,423	1,048	666	288	0
6	1,957	1,556	1,158	760	369	0
7	1,883	1,491	1,110	725	340	0
8	1,986	1,504	1,213	825	440	19
9	2,008	1,608	1,217	829	440	23
10	1,928	1,543	1,167	789	414	0
11	1,973	1,582	1,194	805	420	16
18	---	---	---	---	---	---

REFERENCES

1. I. C. Whittaker and P. M. Besuner, *A Reliability Analysis Approach to Fatigue Life Variability of Aircraft Structures*, AFML-TR-69-65, Air Force Materials Laboratory, March 1969.
2. Private Communication from Y. F. Cheng of The Boeing Scientific Research Laboratory.
3. R. E. Peterson, *Stress Concentration Design Factors*, John Wiley & Sons, Inc., New York, 1953.
4. J. Schijve and F. A. Jacobs, *Fatigue Crack Propagation in Unnotched and Notched Aluminum Alloy Specimens*, Report NLR-TR M.2128, Nationaal Lucht-en Ruimtevaartlaboratorium, May 1964.
5. W. J. Harris, *Metallic Fatigue*, Pergamon Press, 1961.

Unclassified

Security Classification

DOCUMENT CONTROL DATA - R & D		
(Security classification of title, body of abstract and indexing annotation must be entered when the overall report is classified)		
1. ORIGINATING ACTIVITY (Corporate author)		2a. REPORT SECURITY CLASSIFICATION
The Boeing Company; Commercial Airplane Group P.O. Box 3707, Seattle, Washington 98124		Unclassified
		2b. GROUP
3. REPORT TITLE		
A FEASIBILITY STUDY FOR VERIFICATION OF FATIGUE RELIABILITY ANALYSIS		
4. DESCRIPTIVE NOTES (Type of report and inclusive dates)		
Final Report March 16, 1970 through June 15, 1970		
5. AUTHOR(S) (First name, middle initial, last name)		
I. C. Whittaker, J. J. Gerharz		
6. REPORT DATE	7a. TOTAL NO. OF PAGES	7b. NO. OF REFS
September 1970	85	5
8a. CONTRACT OR GRANT NO.	9a. ORIGINATOR'S REPORT NUMBER(S)	
E33615-68-C-1232	AFML-TR-70-157	
b. PROJECT NO.	9b. OTHER REPORT NO(S) (Any other numbers that may be assigned this report)	
7351	D6-25396	
c. Task No. 735106		
d.		
10. DISTRIBUTION STATEMENT		
This document is subject to special export controls, and each transmittal to foreign governments or foreign nationals may be made only with prior approval of the Air Force Materials Laboratory, Wright-Patterson AFB, Ohio 45433.		
11. SUPPLEMENTARY NOTES		12. SPONSORING MILITARY ACTIVITY
		Air Force Materials Laboratory Wright-Patterson Air Force Base, Ohio 45433
13. ABSTRACT		
<p>Experimental data have been developed and analyzed that provide some substantiation of the analytical concepts used in the fatigue reliability analysis outlined in reference 1. Extreme failure data were derived from constant-amplitude fatigue tests of large panels containing 300 identical and independent details, namely, circular holes. These tests simulate a fleet of separate details under controlled operation.</p> <p>Based on finite element analyses and photoelastic experiments, an acceptable panel configuration was determined, providing a virtually identical stress field around each hole of a large number of equally stressed holes. A Boeing-developed crack monitoring system, which uses conductive paint, detected the cracks when they reached 0.02 in. in length. This permitted the cracked holes to be reworked by oversizing and cold working such that the influence on the stress fields of surrounding holes was kept at a minimum.</p> <p>Estimates of the characteristic life and the log-average life were derived from constant-amplitude fatigue tests of small, single-hole specimens loaded under the same conditions as the large panels and showing a hole stress field identical to that in the large panel. These estimates were used to predict the median time to first failure in the large panel.</p> <p>The constant-amplitude fatigue tests establish the feasibility of testing single specimens with a large number of identically stressed details to examine the time-to-failure distribution characteristics of the population of details.</p>		

DD FORM 1473
NOV 65

Unclassified

Security Classification

Unclassified

Security Classification

14.	KEY WORDS	LINK A		LINK B		LINK C	
		ROLE	WT	ROLE	WT	ROLE	WT
	a. Identical and independent details						
	b. Controlled loading environment						
	c. Hole interaction effects						
	d. Stress variation						
	e. Single-hole specimen						
	f. Multihole panel						
	g. Drill-entry side						
	h. Drill-exit side						
	i. Crack initiation						
	j. Crack detection						
	k. Fatigue performance						
	l. Extremal data						
	m. First failure						
	n. Reliability analysis						

Unclassified

Security Classification